Accepted Manuscript

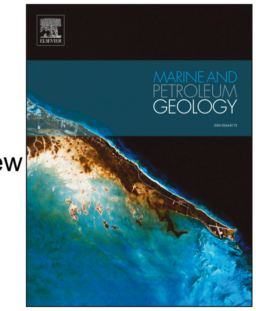

Elongate fluid flow structures: Stress control on gas migration at Opouawe Bank, New Zealand

Michael Riedel, Gareth Crutchley, Stephanie Koch, Christian Berndt, Joerg Bialas, Gerald Eisenberg-Klein, Jürgen Prüßmann, Cord Papenberg, Dirk Klaeschen

PII: S0264-8172(18)30129-6

DOI: 10.1016/j.marpetgeo.2018.03.029

Reference: JMPG 3294

To appear in: *Marine and Petroleum Geology*

Received Date: 16 October 2017

Revised Date: 22 February 2018

Accepted Date: 20 March 2018

Elongate fluid flow structures: Stress control on gas migration at Opouawe Bank, New Zealand

Michael Riedel[1*], Gareth Crutchley[2], Stephanie Koch[1], Christian Berndt[1], Joerg Bialas[1], Gerald Eisenberg-Klein[3], Jürgen Prüßmann[4], Cord Papenberg[1], Dirk Klaeschen[1]

[1] GEOMAR Helmholtz Centre for Ocean Research Kiel, Wischhofstrasse 1 – 3, 24148 Kiel, Germany

[2] GNS Science, 1 Fairway Drive, Avalon 5010, PO Box 30-368, Lower Hutt 5040 New Zealand

[3] TEECware GmbH, Burgwedeler Str. 89, 30916 Isernhagen, Germany

[4] TEEC GmbH, Burgwedeler Str. 89, 30916 Isernhagen, Germany

* corresponding author: mriedel@geomar.de

Keywords:

Gas hydrates, gas migration pathways, 3D seismic attributes, stress control, subduction zone

Abstract

High-resolution 2D and 3D seismic data from Opouawe Bank, an accretionary ridge on the Hikurangi subduction margin off New Zealand, show evidence for exceptional gas migration pathways linked to the stress regime of the ridge. Although the ridge has formed by thrusting and folding in response to a sub-horizontal principal compressive stress (σ_1), it is clear that local stress conditions related to uplift and extension around the apex of folding (i.e. sub-vertical σ_1) are controlling shallow fluid flow. The most conspicuous structural features are parallel and horizontally-elongated extensional fractures that are perpendicular to the ridge axis. At shallower depth near the seafloor, extensional fractures evolve into more concentric structures which ultimately reach the seafloor where they terminate at gas seeps. In addition to the ridge-perpendicular extensional fractures, we also observe both ridge-perpendicular and ridge-parallel normal faults. This indicates that both longitudinal- and ridge-perpendicular extension have occurred in the past. The deepest stratigraphic unit that we image has undergone significant folding and is affected by both sets of normal faults. Shallower stratigraphic units are less deformed and only host the ridge-parallel normal faults, indicating that longitudinal extension was limited to an older phase of ridge evolution. Present-day gas migration has exploited the fabric from longitudinal extension at depth. As the gas ascends to shallower units it 'self-generates' its flow pathways through the more concentric structures near the seafloor. This shows that gas migration can evolve from being dependent on inherited tectonic structures at depth, to becoming self-propagating closer to the seafloor.

1. Introduction

The relationship between gas migration, gas hydrates and seafloor seepage has implications for the understanding of subduction zone processes and the interaction between the global carbon reservoir and seabed ecology. Comprehending the mechanics of fluid migration at subduction zones is important as fluid exerts control on interplate seismogenesis (Ranero et al., 2008). Fluid migration also has a significant impact on the distribution of carbon in the subsurface and the amount of carbon leaking from the seafloor (Berndt, 2005) and thereby cold seep systems (Hovland, 2002; MacDonald et al. 2003; Sibuet und Olu-Le Roy, 2003). Gas seepage from marine sediments comprises a differentiated system from the source and the plumbing structures, to seep structures at the seabed (e.g. Talukder, 2012; Andresen, 2012; Hustoft et al., 2007; Karstens and Berndt, 2015; Løseth et al., 2011; Xu et al., 2018). The migration of fluids or gas can also provide insights into processes of tectonic deformation, the reduction of porosity and compaction of the sedimentary sequences (Aiello, 2005; Bolton and Maltman, 1998); Kvenvolden, 1993).

Plumbing or hydrocarbon leakage systems (Cartwright et al., 2007; Løseth et al., 2009; Løseth et al., 2011; Andresen, 2012) from the reservoir to the seabed are associated with structural migration along faults and fractures or stratigraphically-controlled migration (Talukder, 2012; Plaza-Faverola et al., 2015; Vadakkepuliyambatta et al., 2013). Seismic reflection imaging is an ideal way to investigate the nature of gas-charged fluid migration beneath the seafloor, since focused flow can have profound effects on the reflectivity of sediments. Vertical fluid flow conduits crosscutting the sedimentary strata are often termed seismic pipes or chimneys and usually appear as columnar zones of seismic blanking, turbidity or reduced amplitudes, caused by absorption and scattering of acoustic energy by the gas charged sediments (e.g. Judd and Hovland, 1992; Riedel et al., 2002; Gay et al., 2007; Løseth et al., 2009, Husthoft et al., 2010; Karstens and Berndt, 2015; Plaza-Faverola et al., 2015). Migrating fluids that are expelled at the seabed into the water column are often linked to various seafloor features, such as seep fauna, carbonate precipitates, mud volcanos, pockmarks, mounds and seabed domes (e.g. Hovland and Judd, 1988 and references therein).

On the Hikurangi margin, off New Zealand’s North Island, several areas with multiple seep sites are present (Greinert et al., 2010; Barnes et al., 2010) on the crests of anticlinal ridges situated in 700 - 1200 m water depth. Seeps in these water depths are within the gas hydrate stability zone (GHSZ) and both structurally and stratigraphically controlled fluid migration systems are sustaining the seep sites on these thrust-folded accretionary ridges (Barnes et al., 2010; Crutchley et al., 2010; Krabbenhoeft et al., 2013). At active margins in the accretionary wedge, overpressure is in most cases not sufficient to induce hydrofracturing and fluid flow is mainly initiated by external factors and tectonic stress (Aiello, 2005; Bolton and Maltman, 1998; Talukder, 2012).

In this study we investigate the nature of gas-charged fluid flow beneath Opouawe Bank, an accretionary ridge at the Hikurangi Margin (Figure 1), which is host to 13 seep sites (Greinert et al., 2010). Since these seep sites sustain diverse biological communities and might point to concentrated gas hydrate deposits at depth, we seek to understand which geological conditions favor such focused fluid flow. Using 3D seismic data, our objective is to image and map out the specific structures that allow such prolific gas migration through the gas hydrate layer. Our results will give insight into the local stress conditions beneath the ridge and how they relate to the mechanics of gas migration.

2. Geological setting

The 25 Myr old active Hikurangi Margin off eastern North Island, New Zealand, is the southernmost expression of the Tonga-Kermadec-Hikurangi subduction zone, where westward subduction accommodates oblique convergence between the Pacific Plate and the Australian Plate. At present, the subduction rate is 49 mm/yr at 37°S and declines southwards to 40 mm/yr at 42°S. Southwest of 42°S, strike slip motion begins to dominate (DeMets et al., 2010; Collot et al., 1996; Beavan et al., 2002; Barnes et al., 2010).

Subduction is increasingly more oblique southwards as a result of variation in the plate boundary orientation and the direction of the relative motion between the plates (Wallace et al., 2012). Thus, the margin-normal component of the plate motion decreases southwards and is about 20 mm/yr at the Wairarapa study area (Figure 1), located near the narrowest part of the margin. Most of the margin-normal component is accommodated by the subduction thrust (Barnes and de Lépinay, 1997; Wallace et al., 2012), while the margin-parallel component (about 30 mm/yr in the southern North Island) constitutes strike-slip faulting in the upper plate and forearc block rotation (Beanland and Haines, 1998; Wallace et al., 2004; Wallace et al, 2012).

The accretionary wedge narrows from about 80 km in the central part of the margin to about 13 km at the southern end and thus displays abundant frontal accretion under very oblique convergence. The accretion has led to the formation of right-stepping, thrust-faulted and folded anticlinal ridges parallel to the margin that stand up to 1 km above the surrounding seafloor (Barnes and de Lépinay, 1997). Opouawe Bank, a SW-NE trending oval-shaped bathymetric high, is one of these ridges in the Wairarapa area, culminating in about 1000 m water depth (Barnes et al., 2010). Separated from the continental slope by erosive canyons (Lewis, et al. 1998) and delimited in the south by the Hikurangi Trough (Barnes et al., 2010), the SE flank of Opouawe Bank is characterized by gullies and the NW flank by translational landslide scars (Law et al., 2010). The most recent sediments on the ridge top are hemipelagic mud and turbidity current overspill deposits (Lewis et al., 1998; Luo et al., 2016). The tectonic structure of the Wairarapa area is dominated by three major sub-parallel fault systems; these are, from north to south, the strike-slip Boo Boo Fault, and the Opouawe-Uruti and Pahaua thrust faults (Barnes and de Lépinay, 1997; Barnes et al., 2010). These faults separate the major topographic elevations named Palliser Bank, Pahaua Bank, and Opouawe Bank from each other (Mountjoy et al., 2009).

Opouawe Bank is situated at the northern margin of the Pegasus Basin, which itself is a thick (~9000 m) succession of Albian-Recent sediments that have accumulated south and east of the actively deforming Hikurangi margin (Bland et al., 2015). Large areas of the Pegasus Basin south of Opouawe Bank were explored for oil and gas by Anadarko Petroleum Company from early 2013 until December 2016, at which time the company relinquished its exploration permit. Possible source rocks in the region include marine shales from the Late Cretaceous Whangai Formation and the Late Palaeocene Waipawa Formation (Uruski and Bland, 2011). Gas accumulations are widespread throughout the basin and northwards into the accretionary wedge (Plaza-Faverola et al. 2012; Crutchley et al. 2015). Although Petroleum systems modelling indicates the potential for thermogenic gas generation and migration (Kroeger et al. 2015), gas compositions from gravity cores at Opouawe Bank indicate a purely biogenic source for gas that is migrating through the GHSZ (Koch et al. 2015). The two closest offshore petroleum exploration wells to this study are ‘Tawatawa-1’ and ‘Titihaoa-1’, which lie more than 150 km to the northeast and in water depths that are well inboard of the gas hydrate system. Highly-deformed strata within the wedge and large offsets across thrust ridges preclude any seismic stratigraphic ties from these wells into our study area.

Opouawe Bank lies entirely within the GHSZ, and multi-channel seismic (MCS) data show a bottom simulating reflection (BSR) underlying the flanks in the southwest and northeast and beneath the crest (Netzeband et al., 2010; Plaza-Faverola et al. 2012; Krabbenhoeft et al., 2013). Acoustic manifestations of the subsurface gas migration structures from MCS data have been reported by a number of authors (e.g. Law et al., 2010; Netzeband et al., 2010; Plaza-Faverola et al., 2012; Krabbenhoeft et al. 2013; Koch et al., 2015); the general mechanism of methane migration through the GHSZ at Opouawe Bank was described as structurally controlled (Law et al., 2010; Krabbenhoeft et al., 2013) and Law et al. (2010) concluded that fluid venting is promoted by geological features that include extensional faults, fracture networks and particular stratigraphic pathways. The source depth of the biogenic methane that feeds the seep sites is about 1500-2100 meters below the seafloor (Koch et al., 2016) and the upward migration of methane is influenced by anticlinal focusing (Law et al., 2010). In the upper 100 m below the seafloor, different evolutionary stages in individual gas migration structures and gas-controlled seafloor doming have been reported (Koch et al., 2015).

3. Methods

Reflection seismic data were acquired during the Nemesys Project aboard R/V SONNE (expedition SO214, Bialas et al., 2011). The seismic source was a single 210 in^3 GI gun operated in harmonic mode with a shot interval of 5s. The frequency spectrum of the fully processed 3D data is 30-240 Hz. The recording system was GEOMAR's 3D P-cable system consisting of 16 parallel towed streamers (8 channels each, group spacing of 1.5 m) at a cross-distance of 12.5 m. Thus, the receiver spread (spanning 200 m x 12 m) could measure a footprint of 100 m x 6 m. With a sail line spacing of 50 m, the 3D P-cable survey covers an area of 3 km x 8 km. Additionally, a 2D survey configuration with one 200 m (128 channels at 1.5 m) long streamer was used with the same source to acquire a set of 2D seismic profiles. The main processing steps for the reflection seismic data included navigation correction for source and receiver positions, trace editing, frequency and velocity filtering. The 2D profiles were binned along a crooked line with cell size of 1.5 m. After stacking with water velocity, a Kirchhoff post-stack time migration was applied using a representative velocity function derived from a 2D multichannel seismic line crossing the study region (location see Figure 1). The regional MCS velocities were further extrapolated across the 3D data coverage area accounting for bathymetric changes in the seafloor as well as the depth of the BSR (Schröder, 2013; Koch et al., 2013). The P-cable 3D data were then migrated based on the velocity cube using a full 3D FX time migration algorithm. The very small offset-to-depth ratio of the 2D and 3D data justified using a constant water velocity for stacking prior to migration due to insignificant travel time move-out.

The 3D seismic data processing included an additional "deghosting", specifically developed for the P-Cable acquisition (see Appendix). This process was applied before migration of the 3D data. Binning and stacking in a regular 3D grid with a cell size of 3.125 x 3.125 m provided the input for time migration and subsequent similarity/coherency processing.

To aid seismic interpretation, we calculated similarity volumes from the 3D seismic data using the RockSolid attribute package (Taner, 2003) within Kingdom Suite (IHS; www.ihs.com/products/kingdom-seismic-geological-interpretation-software.html). The similarity is the coherence of each trace over a defined window length (in our case chosen to be 40 ms) and was computed by comparing the data in a time-window, with data in the equivalent windows of neighboring traces. Hence, similarity highlights discontinuities in the data, such as faults, fractures and unconformities (Chopra and Marfurt, 2007). Elongated structures and faults seen within the 3D data were picked on time-slices of the similarity volume within Kingdom Suite. The various azimuths of these structures were then used to generate rose-diagrams within Matlab.

4. Results

4.1 Sedimentary units

The seismic data (Figure 2) across Opouawe Bank display well-stratified sedimentary units. We defined a total of four stratigraphic units based on the seismic reflectivity pattern and amplitude character. Unit boundaries are unconformities, in part erosional surfaces (e.g. between Unit 2 and Unit 1). The depositional character and tectonic deformation of the sedimentary layers suggest that the lowermost Unit 1 consists of older folded and accreted sediments. Above this unit, all other sedimentary sequences are structurally less deformed and generally suggest depositional styles in the form of contourites.

4.2 Normal faulting

The sediment packages comprising the four stratigraphic units are cut by numerous normal faults. Normal faults within the lower-most Unit 1 show two prominent strike orientations (Figure 3): one set of faults strikes in a NNE-SSW trend whereas a second set strikes in an approximately ridge-parallel orientation (ENE-WSW). Normal faults within Units 2 – 4 strike solely in the ridge-parallel orientation, i.e. from ESE to WNW (Figure 4). Strike orientations of faults within each stratigraphic unit are visualized as rose-diagrams in Figure 5.

The dips of the normal faults are mostly towards the centre of Opouawe Bank, i.e. to the NW at the seaward limit, or to the SE at the landward limit of the ridge. The normal faults also cut through all stratigraphic units, and at the SE corner of the ridge they can be traced to below the depth of the BSR. The normal faults are, however, not associated with any amplitude anomalies along the fault traces, e.g. low-amplitude wipe-out zones or bright spots. No gas seeps can be seen at the breaching point of the normal faults with the seafloor. In order to further demonstrate the existence of normal faults across all stratigraphic units, we extracted horizon slices along characteristic layers seen across the 3D data coverage. These horizon slices are shown in the Appendix.

4.3 Seismic wipe-out structures and gas migration pathways

Vertical gas migration pathways, originating in stratigraphic Unit 1, appear as seismic wipe-out zones that can be seen piercing through all overlying sedimentary units (Figure 2). However, in some incidences, the sequence boundary between Units 3 and 4 is a barrier for the pathways (e.g. Figure 2b), and bright-spots develop underneath the unconformity. Within the time-migrated seismic data, wipe-out zones are often associated with reflection pull-ups in the otherwise mostly sub-horizontal sedimentary strata of the shallower parts of the ridge. Due to a lack of detailed velocity control within these zones, we did not convert the time-migrated data to depth to further investigate the nature of these structures and the origin of apparent pull-up.

The spatial relationship between the seep sites (defined at the seafloor) and the gas migration structures within the sediments is best visualized using time-slices through the similarity data volume, compared to the similarity of the seafloor reflection (Figure 6). The similarity time-slices (Figure 6) reveal that the acoustic wipe-out zones at depth are elongated structures that generally strike in the same direction, perpendicular to the trend of the ridge axis (Figure 5).

It is not clear where within Unit 1 the root of these structures is located. Some of them extend beneath the base of the gas hydrate stability zone (or BSR), as visible in Figure 2b. However, underneath the seep structures at the crest of the ridge (Figure 2a) we cannot resolve the structures underneath the base of the gas hydrate stability zone due to accumulation of ascending gas.

The lateral extent of the elongated low-similarity zones beneath the seep sites Piwakawaka, Riroriro, Pukeko, and North Tower can be traced perpendicular to the ridge over lateral distances as great as 1500 m (Figure 6). The orientation of the elongated low-similarity zones does not vary from depth to near the seafloor (Figure 5, 6) where these features are no longer imaged (see Section 4.4 for details).

Gas migration along the elongated zones can be seen in form of bright spots that develop throughout the sedimentary succession above the BSR. The bright spots are short (< 100 – 200 m wide) amplitude anomalies on individual seismic lines (e.g. Figure 2b) but are aligned parallel to the low-similarity elongated structures. Beneath the Riroriro vent site, a gas-related bright spot extends over a distance of ~750 m parallel to the low-similarity zone, with a width of ~100 m, as seen on a time slice at 1.575 s two-way time (Figure 7). Similarly, gas is aligned to both sides of low-similarity fracture zones at the same depth beneath the Pukeko vent site (Figure 8). The gas migrating upward has entered sedimentary layers, but the gas has not migrated laterally over a significant distance, but rather stays closely aligned to the fracture zones. The 3D seismic data show that gas migrates through the elongated structures and spreads out laterally closer to the seafloor, (e.g. Figure 7c, 8c and 9).

4.4 Transition from elongated to rounded gas migration structures

At shallow depths (between 20 – 30 mbsf), the elongated structures can no longer be seen seismically. However, the seismic data show zones of low similarity which are broader, almost rounded, patches close to the seafloor (Figure 9). The structural change of the pathways does not take place at a specific stratigraphic horizon nor at a constant depth below seafloor, and appears to be different at each vent site (Table 1). We report (a) the approximate depths below each vent where a transformation from predominantly elongated to more-dispersed migration pathways are detectable and (b) the depths where this transformation is completed, resulting in an almost circular pattern of low seismic similarity. We convert both depths to hydro- and lithostatic pressures as well as the effective pressure (defined as the difference between litho- and hydrostatic pressure).

The shallow gas migration structures show signs of gas accumulation (Koch et al., 2015). These include gas trapping beneath relatively low-permeability horizons, overpressure accumulation, sediment doming and the subsequent development of methane seep sites. The pressure from a rising gas column resulting in doming and flexural bending of sedimentary layers was estimated to be in the order of 0.4 MPa at the Takahe vent, and 0.5 – 1.1 MPa at the Pukeko vent (Koch et al., 2015). At the seafloor, the seep sites extend laterally for 250 to 500 m (Klaucke et al., 2010). The similarity slice of the seafloor (Figure 6a) shows the surface texture at the seeps. The incoherent nature of the seafloor reflection around the seep sites is the result of carbonate precipitates, which have been described from sidescan sonar data (Dumke et al., 2014; Klaucke et al., 2010).

5. Discussion

5.1. The nature of the elongated seismic anomalies

Gas migration through vertical conduits at Opouawe Bank has been documented previously (Klaucke et al., 2010; Netzeband et al., 2010; Krabbenhoeft et al., 2013; Koch et al., 2015). Although these previous studies lacked the spatial information provided by the 3D survey, Krabbenhoeft et al. (2013) showed that chimney structures are offset with respect to the seeps observed at the seafloor.

The similarity and amplitude time-slices through the 3D data volume (Figure 6, 7, 8) clearly show that the acoustic wipe-out structures in Opouawe Bank are elongated with the long dimension perpendicular to the strike of the ridge at depths greater than 100 ms TWT below the seafloor (Figure 5). Thus, gas migration through Opouawe Bank occurs along parallel elongated pathways, which is unusual as vertical fluid migration structures are usually concentric or elliptic (e.g. Husthoft et al., 2010). However, elongated pathways have been described for a conjugate Riedel shear zone at Omakere ridge, further north on the Hikurangi margin (Plaza-Faverola et al., 2014) and were described in a similar setting off northern Cascadia (Riedel et al., 2002). We propose that elongation of the fluid migration structures is the result of the local stress regime within the anticlinal ridge, meaning that the shape of the fluid migration structures can provide information about the stress pattern.

5.2. Implications for the stress regime

On the margin scale, the relative motion between the Pacific and Australian plates is oriented approximately WSW-ESE (or striking at ~280°) (Figure 1) at the southern end of the Hikurangi subduction zone. Here, the margin-parallel component is accommodated by strike-slip faulting in the upper plate and by forearc block rotation (Beanland and Haines, 1998; Wallace et al., 2004; Wallace et al, 2012). The margin-normal component is mostly accommodated by the subduction thrust (Barnes and de Lépinay, 1997; Wallace et al., 2012). Opouawe Bank is one of the thrust-faulted and folded anticlinal ridges parallel to the margin (Figure 1). Thus, the principal compressive stress at depth beneath Opouawe Bank is most likely perpendicular to the ridge axis – i.e. aligned in a NNW-SSE direction.

Formation of anticlinal ridges of limited lateral extent also leads to secondary longitudinal extension of the ridge due to gravitational forces and the flexure of the ridge (e.g. López et al., 2010, Riedel et al., 2016a). Weinberger and Brown (2006) showed that in the upper 200 – 400 mbsf local forces control the stress state of Southern Hydrate Ridge – i.e. a sub-vertical greatest principal stress (σ1). They infer that the topographic expression of the anticline structure controls this local stress state within the ridge, which drives extension. Similar observations were made from borehole breakouts off northern Cascadia (Riedel et al., 2016b). Extensional fracture alignment in a margin-normal sense (identical in nature to our observations at Opouawe Bank) accompanied with normal faulting parallel to the margin was also described based on P_S splitting analysis along the northern Cascadia deformation front (Tonegawa et al., 2017).

At Opouawe Bank the direction of longitudinal extension is oriented along the ridge axis in an ENE-WSW direction (Figure 5). Hence, the origin of the elongated gas migration structures in a NNW-SSE direction, cutting through all sedimentary units, is most likely the consequence of extensional faults and fractures developing as structures related to the longitudinal extension of the ridge. Furthermore, normal faulting at the SW flank of Opouawe Bank (Figure 3, 4), gullies at the SE flank, and translational landslide scars at the NW flank (Law et al., 2010) are all evidence of the gravitational forces acting on the ridge. This is similar to Hydrate Ridge and the observations by Weinberger and Brown (2006), where the topography of southern Hydrate Ridge leads to gravitational collapse of its top with similar landforms such as sediment slumping and normal faulting on its eastern flank. Therefore, like at Hydrate Ridge, it appears that the greatest principal stress at Opouawe Bank rotates from sub-horizontal on a regional scale to become sub-vertical at the ridge top.

One of the most intriguing observations within Opouawe Bank is the existence of two distinct orientations of normal faults (approximately ridge-perpendicular and ridge-parallel) in Unit 1, relatively deep beneath the seafloor in the most intensely-folded strata. The ridge-perpendicular normal faults that only occur within Unit 1 are an expression of the longitudinal extension that is also manifested in the elongated extensional fractures. The absence of these ridge-perpendicular normal faults in the overlying units indicates that this phase of longitudinal extensional deformation probably ceased prior to the deposition of Units 2, 3 and 4. The ridge-parallel normal faults, striking the same as the axis of folding within Unit 1, appear to be an expression of flexural extension caused by folding. The persistence of these ridge-parallel normal faults to shallower depths (i.e. occurring not only within Unit 1, but also in Units 2 and 3) indicates that flexural extension of the ridge continued to a later stage than the longitudinal extension. Present day gas migration from Unit 1 (and possibly deeper) exploits the ridge-perpendicular fabric caused by longitudinal extension.

5.3. Shallow focusing of fluid flow conduits

At approximately 20 - 30 mbsf, the gas migration structures are no longer elongated but have changed into more circular pathways that culminate in ~circular seep structures (Klaucke et al., 2010, Dumke et al., 2014). The transition starts at sub-seafloor depths varying from 60 to 120 mbsf. As this change in geometry does not take place at a specific stratigraphic horizon, we conclude that it must be controlled by processes that depend on depth beneath the seafloor. The change from elongated to ~circular migration occurs more than 200 m above the base of the gas hydrate stability zone. Therefore, it is unlikely that the presence or absence of gas hydrates (which can strengthen the sediment matrix) causes this transition. Instead we propose that at some shallower sub-seafloor depth, the buoyancy force of free gas becomes more important for gas migration than the influence of existing tectonically-derived structures and local stresses and that the process of gas accumulation, overpressure build-up, doming, and eventually gas break-through forms the approximately circular structures (Koch et al., 2015). With decreasing depth beneath the seafloor, the difference between hydrostatic pressure and lithostatic pressure of the overlying sediment column generally decreases. Gravity cores taken in the region show an average bulk density of 1765 kg/cm^3 (Bialas et al., 2007; Koch et al., 2015), yielding effective pressures at the depths where the transition starts ranging from 0.4 to 0.85 MPa (Table 1). At the depths where the transition is completed to circular structures, the effective pressure ranges from 0.09 to 0.23 MPa. These effective pressures are maximum values, as the actual in situ pore pressure acting on the system is unknown. However, the magnitude of these pressures are within the range of values calculated by Koch et al. (2015) required for gas pockets to form doming structures beneath these vents. Thus, it is conceivable that gas pressure may be high enough to overcome the local effective pressures and create their own buoyancy-driven pathways to the seafloor, unconstrained by any of the regional stresses and stratification.

We therefore propose that the gradual lowering of the differential stress (σ_1 - σ_3) is the dominant mechanism behind the de-focusing of flow; i.e. from elongated flow into sub-circular features. That is, the upward pressure driven by buoyancy of the gas can exceed the confining pressure without the need for large-scale structures (i.e. the elongated fractures seen at greater depths), meaning that buoyancy-driven gas migration dominates.

5.4. Diversity of seep structures at the Hikurangi margin

Numerous active cold seeps occur on the crests of major accretionary ridges at the Hikurangi subduction margin (Greinert et al., 2010; Barnes et al., 2010). At Omakere Ridge, different fluid migration systems exist, affected by shear, compression and extension in a complex deformation regime (Plaza-Faverola et al., 2014). Plaza-Faverola et al. (2014) identified four gas migration systems, with two linked to seafloor seepage. One system was described as closely spaced parallel conduits with elliptical shapes that they referred to as chimneys. These structures are similar to a certain degree to the observed structures on Opouawe Bank, but the structures at Omakere Ridge were interpreted to be conjugate Riedel shear zones rather than zones of extensional fracturing. Normal faulting at Omakere Ridge, at least within the area imaged by 3D seismic data, appears to be limited to ~ridge-parallel faults that have formed in response to flexural extension of the ridge crest (Plaza-Faverola et al. 2014). These ridge-parallel normal faults are therefore similar to those we identified beneath Opouawe Bank. Unlike at Opouawe Bank, the 3D seismic data from Omakere Ridge did not reveal ridge-perpendicular extensional faults. However, extensional structures perpendicular to the strike of accretionary ridges (although without associated gas migration) have been observed at the northern Cascadia margin, where parallel normal faults resulting from longitudinal extension have formed in the direction of the least compressive stress (López et al., 2010; Riedel et al., 2016b).

Rock Garden is another ridge further north on the Hikurangi margin that is influenced by uplift and extension. Crutchley et al. (2010) showed that gas migration beneath Rock Garden is connected to structural deformation, sedimentary fabrics and the gas hydrate phase boundary. The different seep sites are charged either through faults and chimneys, or along the underside of the gas hydrate stability zone, or along highly permeable layers that pass through the GHSZ. Generally, gas migration beneath Rock Garden appears to take place along a northwest-dipping sedimentary fabric.

The wide variety of structural styles found at Opouawe Bank, Omakere Ridge, and Rock Garden demonstrates the variability of geological processes and local stress regimes that influence fluid flow within a subduction zone. Our observation of elongate fluid migration structures is rare in a global context, but as few high-resolution 3D seismic datasets exist in the public literature at active subduction zones it is possible that such structures are more common than thought.

5.5. Implications for petroleum exploration

The widespread occurrence of gas in the Pegasus and East Coast basins has attracted much petroleum exploration, in particular since 2013. Because these basins straddle the active Hikurangi subduction margin, any future exploration or production drilling will require careful consideration of both regional and local tectonic stress regimes, as well as pore fluid pressure. Strong gas-shows and high fluid pressures in East Coast wells underscore both the petroleum potential and exploration safety issues (Darby and Funnell, 2001; Uruski et al. 2005). It is unknown to what extent the deformation fabrics of Opouawe Bank could be representative of other accretionary ridges on this part of the margin, such as the close-by Pahaua Ridge and Palliser Bank. We speculate that similar deformation fabrics probably occur at these ridges, but 3D seismic data would be required to test this inference.

Results of this study have important implications for understanding local stress fields and fluid migration, and how they evolve with depth beneath the seafloor. The two dominant sets of normal faults we identified show how accretionary ridges like Opouawe Bank, in a deforming accretionary wedge, can undergo both ridge-parallel and ridge-perpendicular extension. The fact that just the ridge-parallel faults are currently exploited for focused fluid flow provides new insight into the orientation of the local stress tensor beneath the ridge. The elongated fluid flow structures at depth also highlight the fundamental role of tectonic stress in generating migration pathways; it is only at relatively shallow depths beneath the seafloor that these structural fabrics are abandoned in favor of narrow, circular or sub-circular, focused flow pathways that are maintained by gas pressure. More generally speaking our study shows how high-resolution 3D seismic data can provide constraints on the local stress field without the need for drilling and conducting break-out tests. As such analysis of tectonic structures visible in high-resolution 3D seismic data can improve drilling safety, and contribute to regional geological models without costly experiments.

6. Conclusions

On a regional scale, the deep stress regime on the Hikurangi margin that drives the formation of anticlines like Opouawe Bank is controlled by oblique subduction of the Pacific Plate underneath the Australian Plate. That is, the greatest compressive stress (σ1) is in a sub-horizontal plane. On a local scale, the stress regime around the top of Opouawe Bank is altered such that σ1 migrates to be sub-vertical. High resolution 3D seismic data from Opouawe Bank reveal that, in this local stress field, normal faults have formed in response to both ridge-perpendicular and ridge-parallel extension. We interpret that bending of layers (i.e. flexural extension) and gravitational forces have contributed to the formation of these extensional fabrics. Present day gas migration through the GHSZ has exploited ridge-perpendicular extensional structures, rather than the ridge-parallel structures.

Our analysis of the gas migration pathways through Opouawe Bank shows that their geometry varies with depth, including the unusual observation of elongated, parallel structures below 75 - 100 mbsf. We conclude that a transition from elongated structures at depth to more concentric structures in the shallower sediments results from the declining differential stress that occurs as depth below seafloor decreases. When differential stress is sufficiently low in the shallow sediments, buoyancy-driven gas migration dominates. In other words, the existing elongated structural pathways at depth (formed by ridge-parallel, 'longitudinal' extension) are required for gas to ascend through the deeper parts of the GHSZ. As the gas reaches shallower sub-seafloor depths, gas buoyancy is able to overcome overburden stresses which results in the generation of more circular migration pathways that extend to the seafloor seep sites.

Our 3D seismic data provide new insight into the complexity of gas migration processes in deforming accretionary ridges. In particular, our results highlight the diminishing importance of inherited tectonic structures for sub-seafloor gas migration as gas gets closer to the seafloor.

Acknowledgements

We thank captain and crew of R/V SONNE for their professional support without which the cruise would not have been as successful. NEMESYS project was financed by the German Federal Ministry for Education and Research under grant No. 03G0214A. 3D data acquisition was supported by GNS Science, New Zealand.

References

Aiello, I.W., 2005. Fossil seep structures of the Monterey Bay region and tectonic/structural controls on fluid flow in an active transform margin. Palaeogeography, Palaeoclimatology, Palaeoecology 227, 124-142.

Andresen, K.J., 2012. Fluid flow features in hydrocarbon plumbing systems: What do they tell us about the basin evolution? Marine Geology, 332-334, 89-108, doi:10.1016/j.margeo.2012.07.006.

Barnes, P., and de Lépinay, B.M., 1997. Rates and mechanics of rapid frontal accretion along the very obliquely convergent southern Hikurangi margin, New Zealand, Journal of Geophysical Research 102, 24931-24952.

Barnes, P.M., Lamarche, G., Bialas, J., Henrys, S., Pecher, I.A., Netzeband, G.L., Greinert, J., Mountjoy, J.J., Pedley, K., Crutchley, G.J., 2010. Tectonic and geological framework for gas hydrates and cold seeps on the Hikurangi subduction margin, New Zealand, Marine Geology, 272, 26-48, doi:10.1016/j.margeo.2009.03.012.

Beanland, S., and Haines, J., 1998. The kinematics of active deformation in the North Island, New Zealand, determined from geological strain rates, New Zealand Journal of Geology and Geophysics 41, 311-323, doi:10.1080/00288306.1998.9514813.

Beavan, J., Tregoning, P., Bevis, M., Kato, T., and Meertens, C., 2002. Motion and rigidity of the Pacific Plate and implications for plate boundary deformation, Journal of Geophysical Research 107, doi:10.1029/2001JB000282.

Berndt, C., 2005. Focused fluid flow in passive continental margins: Philosophical Transactions of the Royal Society A, Mathematical, Physical and Engineering Sciences, 363, 2855-2871, doi: 10.1098/rsta.2005.1666.

Bialas, J., Greinert, J., Linke, P., and Pfannkuche, O., eds., 2007. R/V *Sonne* Fahrtbericht/Cruise Report SO191-New Vents: IFM-GEOMAR Report 9, 191 p.

Bialas, J. (ed.), 2011, FS SONNE Fahrtbericht / Cruise Report SO214 NEMESYS: 09.03.-05.04.2011, Wellington - Wellington, 06.-22.04.2011 Wellington – Auckland, IFM-GEOMAR Report, 47, 174 pp. DOI 10.3289/ifm-geomar_rep_47_2011.

Bland, K.J., Uruski, C.I., Isaac, M.J., 2015. Pegasus Basin, eastern New Zealand: A stratigraphic record of subsidence and subduction, ancient and modern, New Zealand Journal of Geology and Geophysics, 58(4), 319-343, https://doi.org/10.1080/00288306.2015.1076862

Bolton, A., Maltman, A., 1998. Fluid-flow pathways in actively deforming sediments: the role of pore fluid pressures and volume change. Marine and Petroleum Geology 15, 281-297.

Cartwright, J., Huuse, M., and Aplin, A., 2007. Seal bypass systems, AAPG Bulletin 91, 1141-1166, doi:10.1306/04090705181.

Chopra, S., Marfurt, K.J., 2007. Seismic attributes for Prospect Identification and Reservoir Characterization, Geophysical Development Series, No. 11, Society of Exploration Geophysicists, Tulsa, OK, ISBN (print): 978-1-56080-141-2

Collot, J., Delteil, J., Lewis, K., Davy, B., Lamarche, G., Audru, J., Barnes, P., Chanier, F., Chaumillon, E., Lallemand, S., de Lépinay, B.M., Orpin, A., Pelletier, B., Sosson, M., Toussaint, B., Uruski, C., 1996. From Oblique Subduction to Intra-Continental Transpression, Structures of the Southern Kermadec-Hikurangi Margin from Multibeam Bathymetry, Side-Scan Sonar and Seismic Reflection: Marine Geophysical Researches18, 357-381.

Crutchley, G.J., Pecher, I.A., Gorman, A.R., Henrys, S.A., Greinert, J., 2010. Seismic imaging of gas conduits beneath seafloor seep sites in a shallow marine gas hydrate province, Hikurangi Margin, New Zealand, Marine Geology 272, 114-126, doi:10.1016/j.margeo.2009.03.007.

Crutchley, G.J., Fraser, D.R.A., Pecher, I.A., Gorman, A.R., Maslen, G., Henrys, S.A., 2015. Gas migration into gas hydrate-bearing sediments on the southern Hikurangi margin of New Zealand:, 1-19, doi:10.1029/2001.

Darby, D., Funnell, R.H., 2001. Overpressure associated with a convergent plate margin: East Coast Basin, New Zealand, Petroleum Geoscience, 7, 291-299, https://doi.org/10.1144/petgeo.7.3.291

DeMets, C., Gordon, R.G., Argus, D.F., 2010. Geologically current plate motions, Geophysical Journal International, 181, 1-80, doi:10.1111/j.1365-246X.2009.04491.x.

Dumke, I., Klaucke, I., Berndt, C., Bialas, J., 2014. Sidescan backscatter variations of cold seeps on the Hikurangi Margin (New Zealand), indications for different stages in seep development: Geo-Marine Letters 34, 169-184, doi:10.1007/s00367-014-0361-7.

Gay, A., Lopez, M., Berndt, C., Séranne, M., 2007. Geological controls on focused fluid flow associated with seafloor seeps in the Lower Congo Basin, Marine Geology, 244(1-4), 68-92, doi: 10.1016/j.margeo.2007.06.003

Greinert, J., Lewis, K.B., Bialas, J., Pecher, I.A., Rowden, A., Bowden, D.A., de Batist, M.D., de Batist, M., Linke, P., 2010. Methane seepage along the Hikurangi Margin, New Zealand, Overview of studies in 2006 and 2007 and new evidence from visual, bathymetric and hydroacoustic investigations: Marine Geology, 272, 6-25, doi:10.1016/j.margeo.2010.01.017.

Hovland, M., 2002. On the self-sealing nature of marine seeps, Continental Shelf Research 22, 2387-2394, doi:10.1016/S0278-4343(02)00063-8.

Hovland, M., Judd, A., 1988. Seabed pockmarks and seepages, impact on geology, biology, and the marine environment: Springer.

Husthoft, S., Mienert, J., Bünz, S., Nouzé, H., 2007. High-resolution 3D-seismic data indicate focussed fluid migration pathways above polygonal fault systems of the mid-Norwegian margin. Marine Geology 245, 89-106

Husthoft, S., Bünz, S., Mienert, J., 2010. Three-dimensional seismic analysis of the morphology and spatial distribution of chimneys beneath the Nyegga pockmark field, offshore mid-Norway, Basin Research 22, 465-480, doi:10.1111/j.1365-2117.2010.00486.x.

Judd, A.G., Hovland, M., 1992. The evidence of shallow gas in marine sediments, Continental Shelf Research 12, 1081-1095.

Karstens, J., Berndt, C., 2015. Seismic chimneys in the Southern Viking Graben – Implications for palaeo fluid migration and overpressure evolution, Earth and Planetary Science Letters 412, 88-100, doi:10.1016/j.epsl.2014.12.017.

Klaucke, I., Weinrebe, W., Petersen, C.J., Bowden, D., 2010. Temporal variability of gas seeps offshore New Zealand: Multi-frequency geoacoustic imaging of the Wairarapa area, Hikurangi margin, Marine Geology 272, 49-58, doi:10.1016/j.margeo.2009.02.009.

Koch, S., Berndt, C., Bialas, J., Haeckel, M., Crutchley, G., Papenberg, C., Klaeschen, D., Greinert, J., 2015. Gas-controlled seafloor doming, Geology 43, 571-574, doi:10.1130/G36596.1.

Koch, S., Schroeder, H., Haeckel, M., Berndt, C., Bialas, J., Papenberg, C., Klaeschen, D., Plaza-Faverola, A., 2016. Gas migration through Opouawe Bank at the Hikurangi margin offshore New Zealand, Geo-marine Letters, 1-10, doi:10.1007/s00367-016-0441-y

Krabbenhoeft, A., Bialas, J., Klaucke, I., Crutchley, G., Papenberg, C., Netzeband, G.L., 2013. Patterns of subsurface fluid-flow at cold seeps, The Hikurangi Margin, offshore New

Zealand: Marine and Petroleum Geology 39, 59-73, doi:10.1016/j.marpetgeo.2012.09.008.

Kroeger, K.F., Plaza-Faverola, A., Barnes, P.M., Pecher, I.A., 2015. Thermal evolution of the New Zealand Hikurangi subduction margin: Impact on natural gas generation and methane hydrate formation - A model study, Journal of Marine and Petroleum Geology, 63, 97-114, doi:10.1016/j.marpetgeo.2015.01.020.

Kvenvolden, K.A., 1993. Gas Hydrates - Geological Perspective and Global Change: Reviews of Geophysics 31, 173-187, doi:10.1029/93RG00268.

Law, C.S., Nodder, S.D., Mountjoy, J.J., Marriner, A., Orpin, A., Pilditch, C.A., Franz, P., Thompson, K., 2010. Geological, hydrodynamic and biogeochemical variability of a New Zealand deep-water methane cold seep during an integrated three-year time-series study, Marine Geology 272, 189-208, doi:10.1016/j.margeo.2009.06.018.

Lewis, K.B., Collot, J., Lallemand, S.E., 1998. The dammed Hikurangi Trough: a channel-fed trench blocked by subducting seamounts and their wake avalanches (New Zealand–France GeodyNZ Project), Basin Research 10, 441-468, doi:10.1046/j.1365-2117.1998.00080.x.

Luo, M., A. W. Dale, L. Haffert, M. Haeckel, S. Koch, G. Crutchley, H. De Stigter, D. Chen, J. Greinert, 2016. A quantitative assessment of methane cycling in Hikurangi Margin sediments (New Zealand) using geophysical imaging and biogeochemical modeling, Geochem. Geophys. Geosyst., 17, 4817–4835, doi:10.1002/2016GC006643.

López, C., Spence, G., Hyndman, R., Kelley, D., 2010. Frontal ridge slope failure at the northern Cascadia margin: Margin-normal fault and gas hydrate control, Geology 38, 967-970, doi:10.1130/G31136.1.

Løseth, H., Gading, M., Wensaas, L., 2009. Hydrocarbon leakage interpreted on seismic data, Journal of Marine and Petroleum Geology 26, 1304-1319, doi:10.1016/j.marpetgeo.2008.09.008.

Løseth, H., Wensaas, L., Arntsen, B., Hanken, N.-M., Basire, C., Graue, K., 2011. 1000 m long gas blow-out pipes. Marine and Petroleum Geology 28, 1047-1060.

MacDonald, I.R., Sager, W.W., Peccini, M.B., 2003. Gas hydrate and chemosynthetic biota in mounded bathymetry at mid-slope hydrocarbon seeps: northern Gulf of Mexico, Marine Geology, 198, 133–158.

Mountjoy, J.J., Barnes, P.M., Pettinga, J.R., 2009. Morphostructure and evolution of submarine canyons across an active margin: Cook Strait sector of the Hikurangi Margin, New Zealand. Marine Geology 260, 45-68.

Netzeband, G.L., Krabbenhoeft, A., Zillmer, M., Petersen, C.J., Papenberg, C., Bialas, J., 2010. The structures beneath submarine methane seeps: Seismic evidence from Opouawe Bank, Hikurangi Margin, New Zealand, Marine Geology 272, 59-70, doi:10.1016/j.margeo.2009.07.005.

Plaza-Faverola, A., Klaeschen, D., Barnes, P., Pecher, I., Henrys, S., Mountjoy, J., 2012. Evolution of fluid expulsion and concentrated hydrate zones across the southern Hikurangi subduction margin, New Zealand: An analysis from depth migrated seismic data, Geochemistry, Geophysics, Geosystems 13, doi:10.1029/2012GC004228.

Plaza-Faverola, A., I. Pecher, G. Crutchley, P. M. Barnes, S. Bünz, T. Golding, D. Klaeschen, C. Papenberg, J. Bialas, 2014. Submarine gas seepage in a mixed contractional and shear deformation regime: Cases from the Hikurangi oblique-subduction margin, Geochem. Geophys. Geosyst., 15, 416–433, doi:10.1002/2013GC005082.

Plaza-Faverola, A., Bünz, S., Johnson, J.E., Chand, S., Knies, J., Mienert, J., Franek, P., 2015. Role of tectonic stress in seepage evolution along the gas hydrate-charged Vestnesa Ridge, Fram Strait, Geophysical Research Letters, 42, 733–742, doi:10.1002/2014GL062474.

Ranero, C., Grevemeyer, I., Sahling, H., Barckhausen, U., Hensen, C., Wallmann, K., Weinrebe, W., Vannucchi, P., Huene, von, R., and McIntosh, K., 2008. Hydrogeological system of erosional convergent margins and its influence on tectonics and interplate seismogenesis: Geochemistry Geophysics Geosystems 9, 1-18, doi:10.1029/2007GC001679.

Riedel, M., Hyndman, R.D., Spence, G.D., Chapman, N.R., 2002. Seismic investigations of a vent field associated with gas hydrates, offshore Vancouver Island, Journal of Geophysical Research, JGR Solid Earth, Vol 107, No. B9, 2200, doi:10.1029/2001.

Riedel, M., Naegeli, K., Côté, M.M., 2016a. Assessment of slope failures off Vancouver Island, Geological Survey of Canada, Open File 8008, 108p, https://doi.org/10.4095/297904

Riedel, M. Malinverno, A., Wang, K., Goldberg, D., Guerin, G., 2016b. Horizontal compressive stress regime on the northern Cascadia margin inferred from borehole breakouts, Geochemistry, Geophysics, Geosystems, 17, 3529–3545, *doi:*10.1002/2016GC006443

Schröder, H., 2013. Pre stack depth migration of 2D MCS data and velocity field extrapolation on Opouawe Bank, offshore New Zealand, Diploma thesis, Christian-Albrechts-Universität, Kiel, 51 pp.

Sibuet, M., Olu-Le Roy, K., 2003. Cold seep communities on continental margins: Structure and quantitative distribution relative to geological and fluid venting patterns, In: Ocean Margin Systems (eds. G. Wefer, D.S.M. Billett, D. Hebbeln, etal.), 235-251, Berlin: Springer.

Taner, M.T., 2003. Attributes Revisited, Report available online at http://www.rocksolidimages.com/attributes-revisited/ (last visited January 31, 2018).

Talukder, A.R., 2012. Review of submarine cold seep plumbing systems: leakage to seepage and venting, Terra Nova 24, 255-272, doi:10.1111/j.1365-3121.2012.01066.x.

Tonegawa, T., Obana, K., Yamamoto, Y., Kodaira, S., Wang, K., Riedel, M., Kao, H., Spence, G., 2017. Fracture alignments in marine sediments off Vancouver Island from P_S splitting analysis, Bulletin of the Seismological Society of America, Vol. 107, No. 1, 16p, doi: 10.1785/0120160090

Uruski, C.I., Field, B.D., Funnell, R., 2005. The East Coast Basin of New Zealand, an emerging petroleum province, The APPEA Journal, 45(1), 563-580, https://doi.org/10.1071/AJ04043

Uruski, C.I., Bland, K., 2011. Pegasus Basin and then prospect for oil and gas, GNS Science Client report 2010/291 and New Zealand Open-File Petroleum Report 4326. Crown Minerals, Wellington.

Vadakkepuliymbatta, S., Bünz, S., Mienert, J., Chand, S., 2013. Distribution of subsurface fluid-flow systems in the SW Barents Sea. Marine and Petroleum Geology 43, 208-221.

Wallace, L.M., Beavan, J., McCaffrey, R., Darby, D., 2004. Subduction zone coupling and tectonic block rotations in the North Island, New Zealand, Journal of Geophysical Research 109, doi:10.1029/2004JB003241.

Wallace, L.M., Barnes, P., Beavan, J., van Dissen, R.V., van Dissen, R., Litchfield, N., Mountjoy, J., Langridge, R., Lamarche, G., Pondard, N., 2012. The kinematics of a transition from subduction to strike-slip, An example from the central New Zealand plate boundary: Journal of Geophysical Research 117, B02405, doi:10.1029/2011JB008640.

Weinberger, J.L., Brown, K.M., 2006. Fracture networks and hydrate distribution at Hydrate Ridge, Oregon, Earth and Planetary Science Letters 245, 123-136, doi:10.1016/j.epsl.2006.03.012.

Xu, C., Greinert, J., Haeckel, M., Bialas, J., Dimitrov, L., Zhao, G., 2018. The Character and Formation of Elongated Depressions on the Upper Bulgarian Slope. Journal of Ocean University of China 17

Yuan, F., Bennell, J.D., Davis, A.M., 1992. Acoustic and physical characteristics of gassy sediments in the western Irish Sea, Continental Shelf Research 12, 1121-1134

Figure captions

Figure 1. a) Bathymetric map showing the location of Opouawe Bank at the Hikurangi margin, offshore New Zealand. Geological structures are from Wallace et al. (2012). Blue arrow shows the relative plate motion vector of the Australian and Pacific plates at the southern North Island, with most of the margin normal component of the plate motion occurring on the subduction thrust and the margin parallel component as a combination of strike-slip faulting and forearc rotation (Wallace et al., 2012 an references therein). Red arrows display the modeled relative motion (in mm/yr) between tectonic block boundaries in the east and the Pacific plate (Wallace et al., 2012). BBF = Boo Boo Fault; OUF = Opouawe-Uruti Fault; PF = Pahaua Fault. (b) Location of seep sites (white stars) on Opouawe Bank: 1 = Piwakawaka; 2 = Riroriro; 3 = Pukeko; 4 = North Tower; 5 = South Tower; 6 = Takahe; 7 = Takapu; 8 = Tete. The yellow rectangle displays the outline of the 3D seismic volume and the black lines indicate the location of the 2D MCS data (Figure 2).

Figure 2. a) Northern Line 1, b) southern Line 2, both along the main seep sites on Opouawe Bank, and (c) crossing 2D seismic Line 3 perpendicular to (a) and (b) displaying the gas migration pathways through the ridge. These pathways appear as vertical conduits of limited extent on the 2D seismic. Figure 5 displays their spatial structure to be elongated across the ridge. Sequence boundaries are shown as dotted lines. [BSR = Bottom Simulating Reflector]

Figure 3. (a) Amplitude time slice and (b) similarity time slice at 1.834 s (two-way time) showing detailed structure of normal faults within stratigrahic Unit 1 with two sets of strike orientation. Note: for the similarity plot, high coherence is white, low coherence is black. The NNW-SSE trending set of faults are parallel to the more-prominent elongated structures that form the gas migration pathways at the centre of the ridge fold axis. (c) Crossline 2583 depicting stratigraphic units 1 – 4. Red horizontal line is depth of time slice shown in (a) and (b).

Figure 4. (a) Amplitude time slice and (b) similarity time slice at 1.67 s (two-way time) showing detailed structure of normal faults within stratigrahic Units 2 - 4 with only one dominant strike orientation (ENE – WSW). The NNW-SSE trending zones of fracturing (elongated structures) forming gas migration pathways occur at the centre at the ridge. (c) Crossline 2583 depicting

stratigraphic units 1 – 4. Red horizontal line is depth of time slice shown in (a) and (b). Note: for the similarity plot, high coherence is white, low coherence is black.

Figure 5. Rose diagrams depicting the dominant strike direction of normal faults (blue) and elongated structures (black) in all four stratigraphic units. Ridge-strike direction (70-75°) is indicated in grey color. Direction of plate convergence at Opouawe bank is ~280°. The rose diagrams show the statistical spread of azimuthal values of individual fault segments only, not the length of fault segments themselves. Orientations were picked from horizon slices shown in the Appendix.

Figure 6. Comparison of similarity attribute extracted from the 3D seismic data volume over a 40 ms thick window length. a) similarity extracted at the seafloor, b) time slice at 1.64 s two-way time (TWT), (c) time slice at 1.74 s TWT, and (d) time slice at 1.84 s TWT. On all slices, the locations of vent sites as defined from side-scan sonar backscatter imagery (Klaucke et al., 2010) are indicated by red-colored polygons. Sequence boundaries between the units are indicated by yellow dashed lines. Direction of plate convergence at Opouawe bank (~280°) is indicated by black arrow.

Figure 7 Example of gas migration at the Riroriro vent (lateral extent at seafloor defined from backscatter is indicated by red polygon): (a) time slice of reflection amplitude extracted at 1.575 s two-way time showing elongated bright spot (length ~ 750 m, width ~ 100 m) indicating free gas (b), seismic similarity at same depth showing orientation of fluid-flow structure with low similarity striking at ~345°, (c) inline 2311 connecting the four vent sites Piwakawaka in the SE to North Tower in the NW of Opouawe bank.

Figure 8 Example of gas migration at the Pukeko vent (lateral extent at seafloor defined from backscatter is indicated by red polygon): (a) time slice of reflection amplitude extracted at 1.575 s two-way time showing two parallel elongated bright spots (length ~ 330 m, width ~ 50 m) indicating free gas (b), seismic similarity at same depth showing orientation of abroad fluid-flow structure with low similarity striking at ~345°, (c) inline 2311 connecting the four vent sites Piwakawaka in the SE to North Tower in the NW of Opouawe bank.

Figure 9 Near-seafloor distribution of free gas beneath vent sites within 3D seismic data volume visualized by seafloor-parallel slices 20 ms two-way time (~20 meter) of (a) reflection amplitude and (b) seismic similarity. Zones of low similarity and high amplitude are surrounded by black dashed lines indicating a broad and no longer elongated distribution of free gas (and potential carbonate). Lateral extent of the vents at the seafloor as defined from backscatter (Klaucke et al., 2010) are shown by red polygons, further showing an additional focusing and lateral deviation of gas migration. At this depth no elongated structures can be identified, which is in stark contrast to Omakere Ridge (Plaza-Faverola, 2012).

Figure 10. Sketches (not to scale) display Opouawe Bank in relation to the regional tectonic regime (a) and the local stress regime of the ridge (b). The elongated gas migration structures are the result of an anisotropic stress regime within the central portion of the anticlinal ridge. The thrust-faulted and folded accretionary ridge (a) is a result of a sub-horizontal greatest compressive stress (σ_1). Here, over pressure is high, resulting in upward migration of fluids and gas. Ridge-perpendicular and longitudinal extension around the ridge top, which opens pathways for fluid and gas migration, are manifestations of σ_1 rotating to sub-vertical at a local scale.

Appendix 1

Deghosting of the 3D P-Cable Data

Seismic receiver ghost signals of the 3D P-Cable data could not be removed with conventional approaches due to the variable depth of the receivers ranging from nominal 2m down to 8m. The reason for this large variation is a sag of the central part of the cross-cable as well as the connected individual streamers, depending on ship speed and local currents (Figure A1b).

A seismic reflection arriving from below is recorded twice at the P-cable receivers, first as a direct pulse, and after reflection at the sea-surface as a ghost (Figure A1a). The direct pulse reaches the deep central streamers first, and the shallow streamers at the end at last. The receiver ghost wave exhibits the opposite behavior, with a delay proportional to the water depth of the receivers. In a shot recording, both arrivals form bow-shaped events that combine into elliptic pearl-shaped patterns (Figure A1c, d). Crosslines covering several shots show these reflections as "pearl-necklaces" (Figures A2a, b).

The processing strategy to remove these pearl-shaped ghost artifacts is based on an automated identification of the prominent water bottom reflection and analysis of the composite signals formed by direct and ghost reflections. Individual wavelet convolution filters predict and remove the variable ghost signals. Individual time corrections remove the bow-shaped time shifts due to variable receiver depths, thus yielding the desired high data resolution (see comparison of raw data and data with deghosting applied, Figure A2a-d).

Appendix 1 Figures

Figure A1: The sketch a) indicates the separation or interference of seismic source signals with its ghost reflections from the sea surface on the source and receiver sides, with dependence on the depth of the receiver. The streamer depths of a shot recording vary according to the blue curve in b) which causes a systematic pattern. This is more obvious in the shot recording c) with the seismic signals from all 128 channels, where each group of 8 channels belongs to an individual streamer. The combined signals of adjacent shots produce the ‘pearl-necklace’ pattern d), which is also visible in the stacked cube shown in Fig. A2.

Figure A2: The benefit of the special deghosting is most obvious in the comparison of stacked time sections (inline 2030) a) before and b) after the deghosting, where the ‘pearl-necklace’ structures indicated by the arrows have been removed. Also the footprint, clearly visible in the time-slice view (taken at 1.2 s two-way time) of the 3D data cube c) before deghosting, is efficiently reduced in the corresponding time-slice d) after deghosting.

Appendix 2

Horizon slices extracted from each of the four stratigraphic units.

Figure A3 Crossline 2508 depicting location of horizons within the four units. Boundaries between the units are shown by black dashed lines. A mass-transport deposit (MTD) is seen at the NE corner of the data. The bottom-simulating reflector (BSR) at the base of the gas hydrate stability field is indicated by a dotted line.

Figure A4 Horizon slice of a layer (a) within Unit 1, and (b) within Unit 2.

Figure A5 Horizon slice of a layer (a) within Unit 3, and (b) within Unit 4.

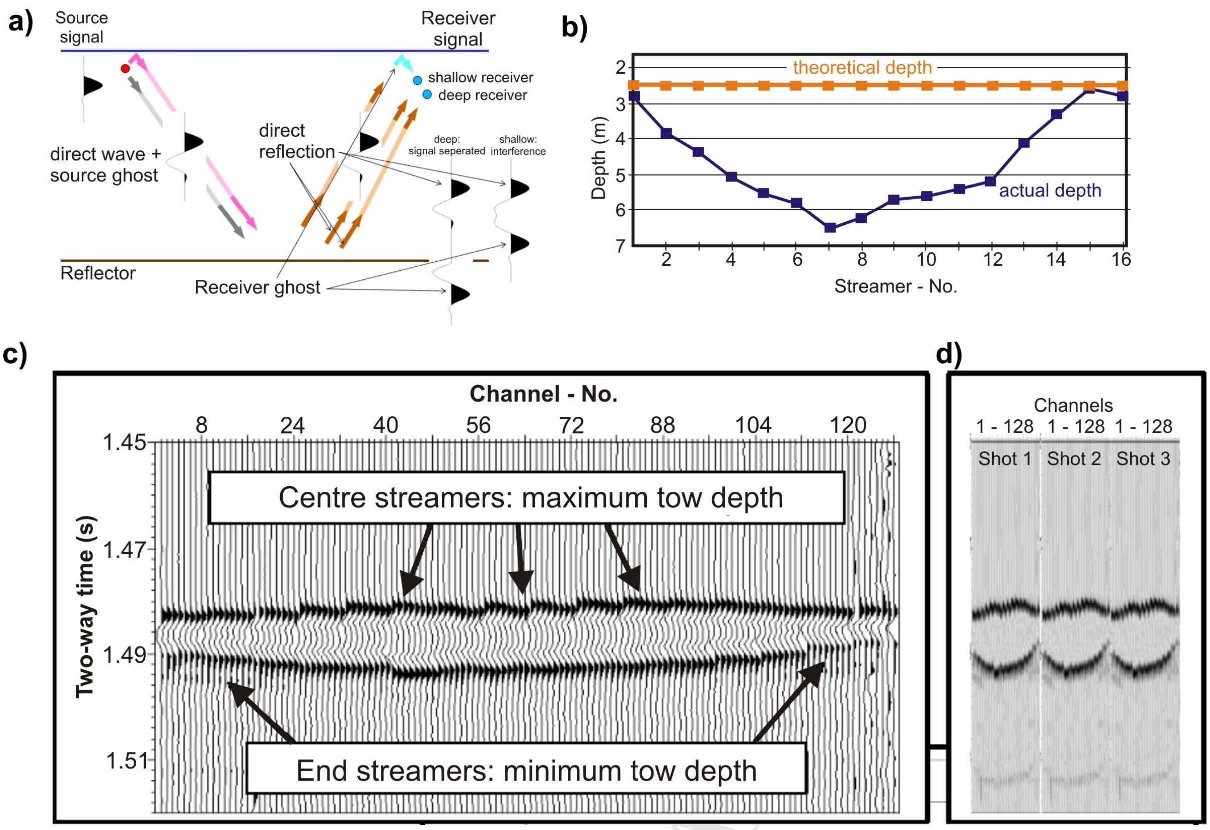
a)
Source signal
Receiver signal
shallow receiver
deep receiver
direct wave + source ghost
direct reflection
deep: signal seperated
shallow: interference
Reflector
Receiver ghost
b)
theoretical depth
actual depth
Depth (m)
Streamer - No.
c)
Channel - No.
Two-way time (s)
Centre streamers: maximum tow depth
End streamers: minimum tow depth
d)
Channels
1 - 128
1 - 128
1 - 128
Shot 1
Shot 2
Shot 3

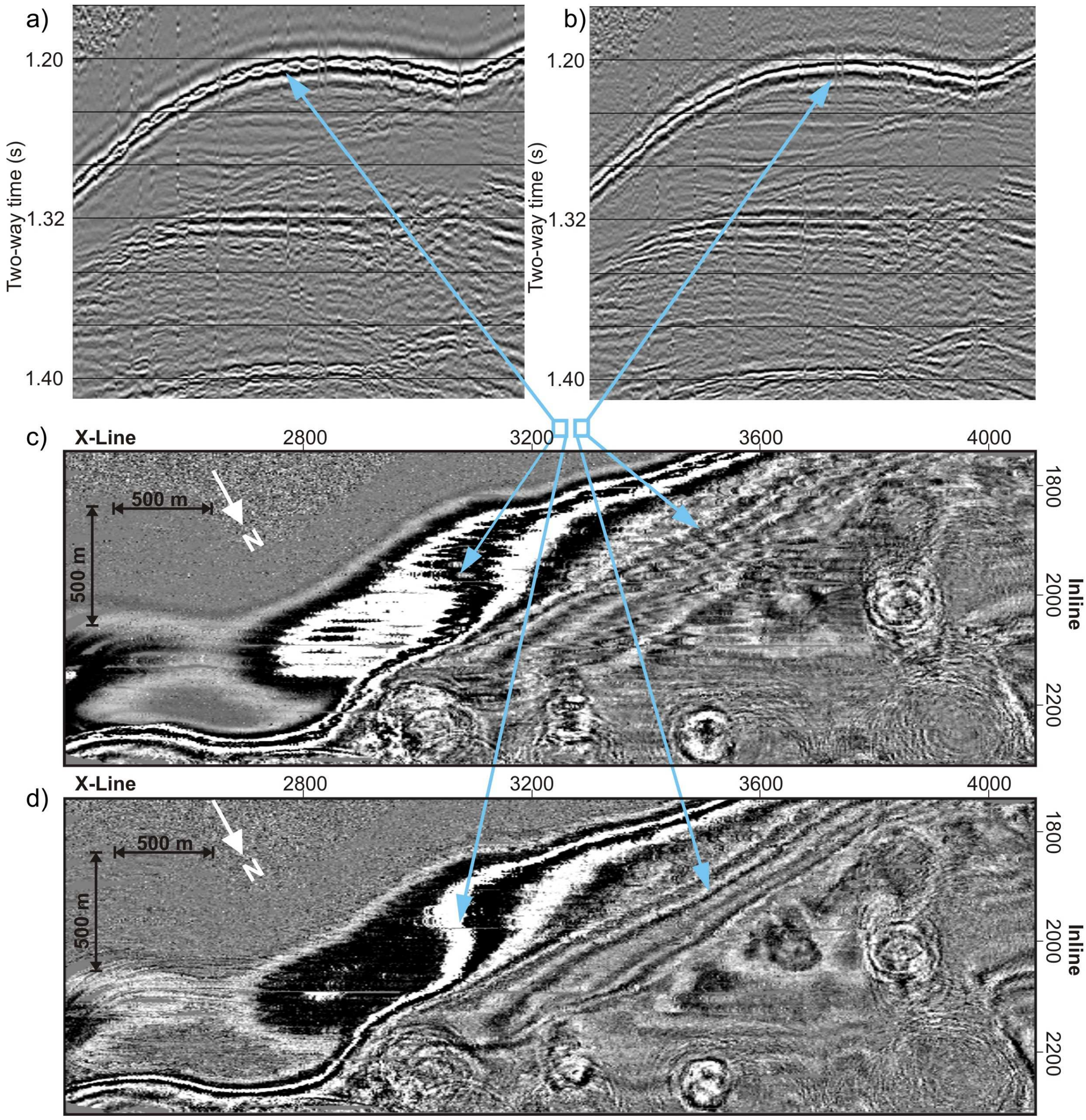
a)
b)
1.20
1.32
1.40
Two-way time (s)
c)
d)
X-Line
2800
3200
3600
4000
1800
2000
2200
Inline
500 m
500 m
N

Table 1 Depths of transition from elongated to sub-rounded (i.e. ~equal width-length ratios) gas migration pathways at the five vent sites imaged within the 3D P-cable data (measured in ms two-way time (TWT) and converted to meters below seafloor (mbsf) using a constant velocity of 1550 m/s at shallow depth and 1600 m/s for greater depths, based on the 3D velocity model used for migration). We defined lithostatic pressure (P_{lith}) using an average sediment bulk density of 1765 kg/m^3 (Bialas et al., 2007; Koch et al., 2015) and hydrostatic pressure (P_{hyd}) using a water density of 1030 kg/m^3.

Vent Site	Piwakawaka	Riroriro	Pukeko	North Tower	South Tower
Water depth (m)	1085	1060	1045	1035	1040
Depth at start of transition (ms / mbsf)	71 / 57	116 / 93	147 / 118	68 / 54.5	105 / 84
Depth of completed transition (ms / mbsf)	42 / 32.5	27 / 21	37 / 28.5	34 / 26	25 / 19.5
P_{hyd} at start of transition (10^6 Pa)	11.54	11.65	11.75	11.01	11.36
P_{lith} at start of transition (10^6 Pa)	11.95	12.32	12.60	11.40	11.96
(P_{lith} - P_{hyd}) at start of transition (10^6 Pa)	0.41	0.67	0.85	0.39	0.6
P_{hyd} at complete transition (10^6 Pa)	11.29	10.92	10.85	10.72	10.76
P_{lith} at complete transition (10^6 Pa)	11.52	11.07	11.05	10.91	10.85
(P_{lith} - P_{hyd}) at complete transition (10^6 Pa)	0.23	0.15	0.2	0.19	0.09

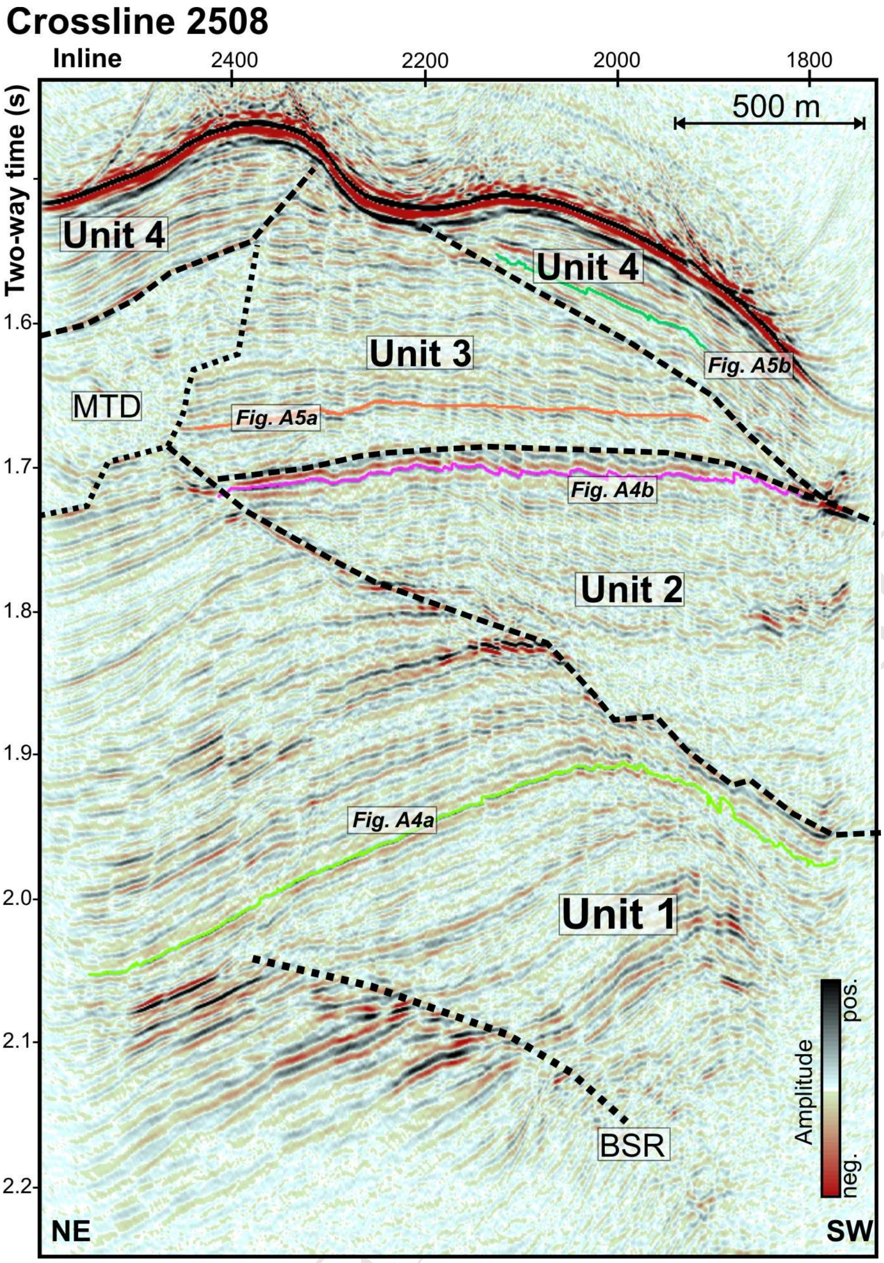
Crossline 2508
Inline
2400
2200
2000
1800
500 m
Two-way time (s)
1.6
1.7
1.8
1.9
2.0
2.1
2.2
Unit 4
Unit 4
Unit 3
Unit 2
Unit 1
MTD
Fig. A5a
Fig. A5b
Fig. A4b
Fig. A4a
BSR
Amplitude
pos.
neg.
NE
SW

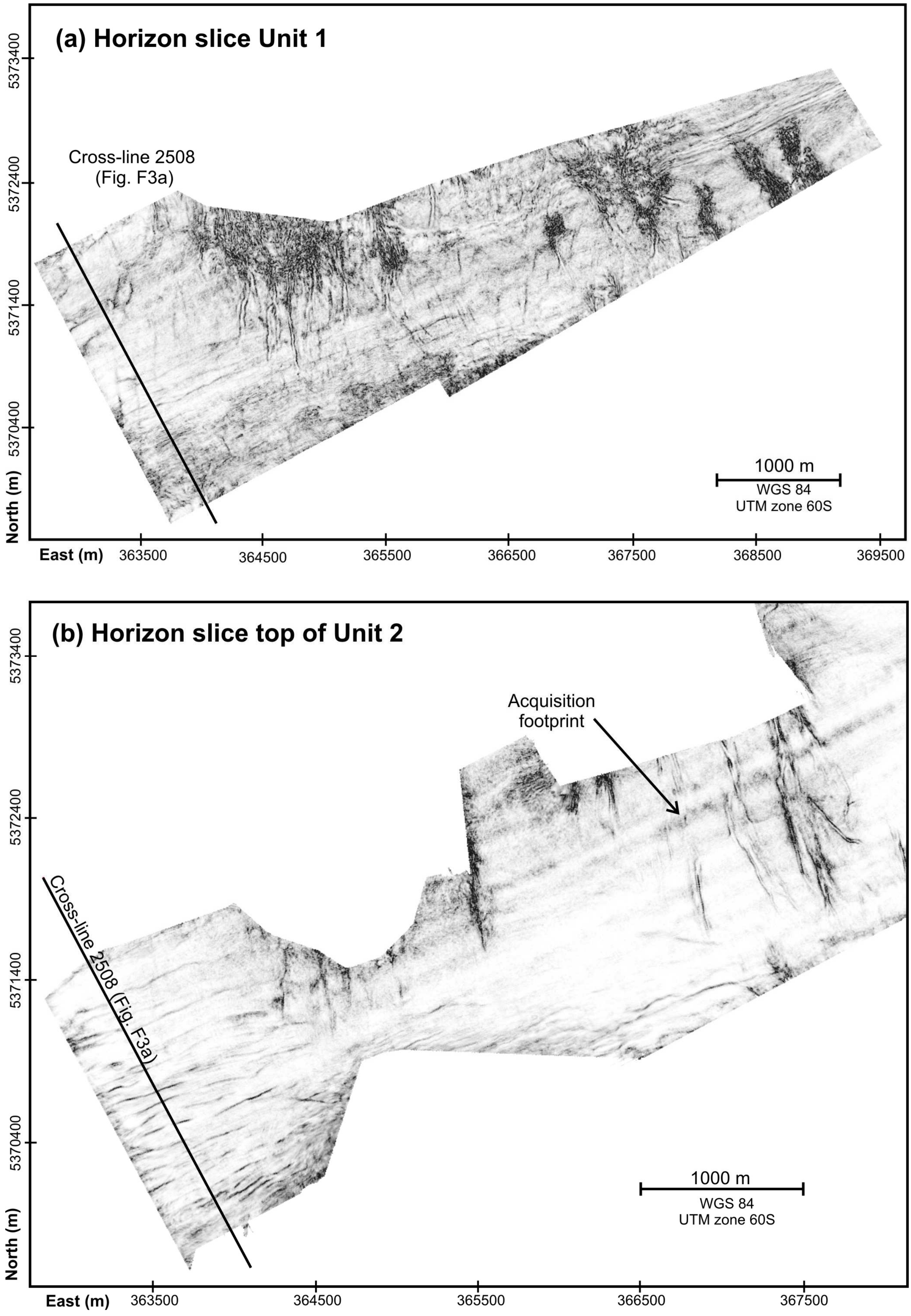
(a) Horizon slice Unit 1
Cross-line 2508
(Fig. F3a)
1000 m
WGS 84
UTM zone 60S
North (m)
5373400
5372400
5371400
5370400
East (m)
363500
364500
365500
366500
367500
368500
369500
(b) Horizon slice top of Unit 2
Acquisition
footprint
Cross-line 2508 (Fig. F3a)
1000 m
WGS 84
UTM zone 60S
North (m)
5373400
5372400
5371400
5370400
East (m)
363500
364500
365500
366500
367500

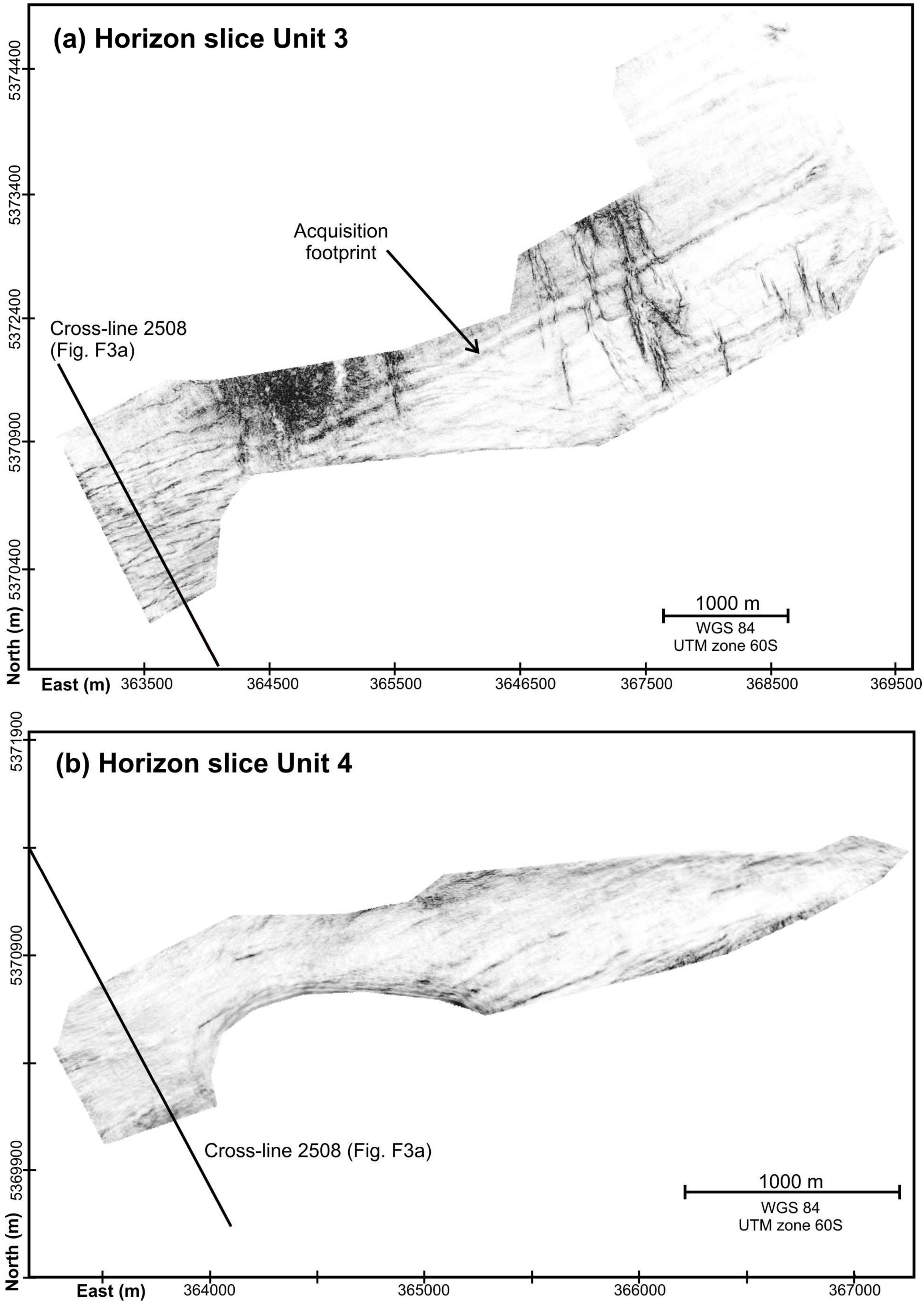
(a) Horizon slice Unit 3
Acquisition footprint
Cross-line 2508 (Fig. F3a)
1000 m
WGS 84
UTM zone 60S
North (m)
5374400
5373400
5372400
5370900
5370400
East (m)
363500
364500
365500
3646500
367500
368500
369500
(b) Horizon slice Unit 4
Cross-line 2508 (Fig. F3a)
1000 m
WGS 84
UTM zone 60S
North (m)
5371900
5370900
5369900
East (m)
364000
365000
366000
367000

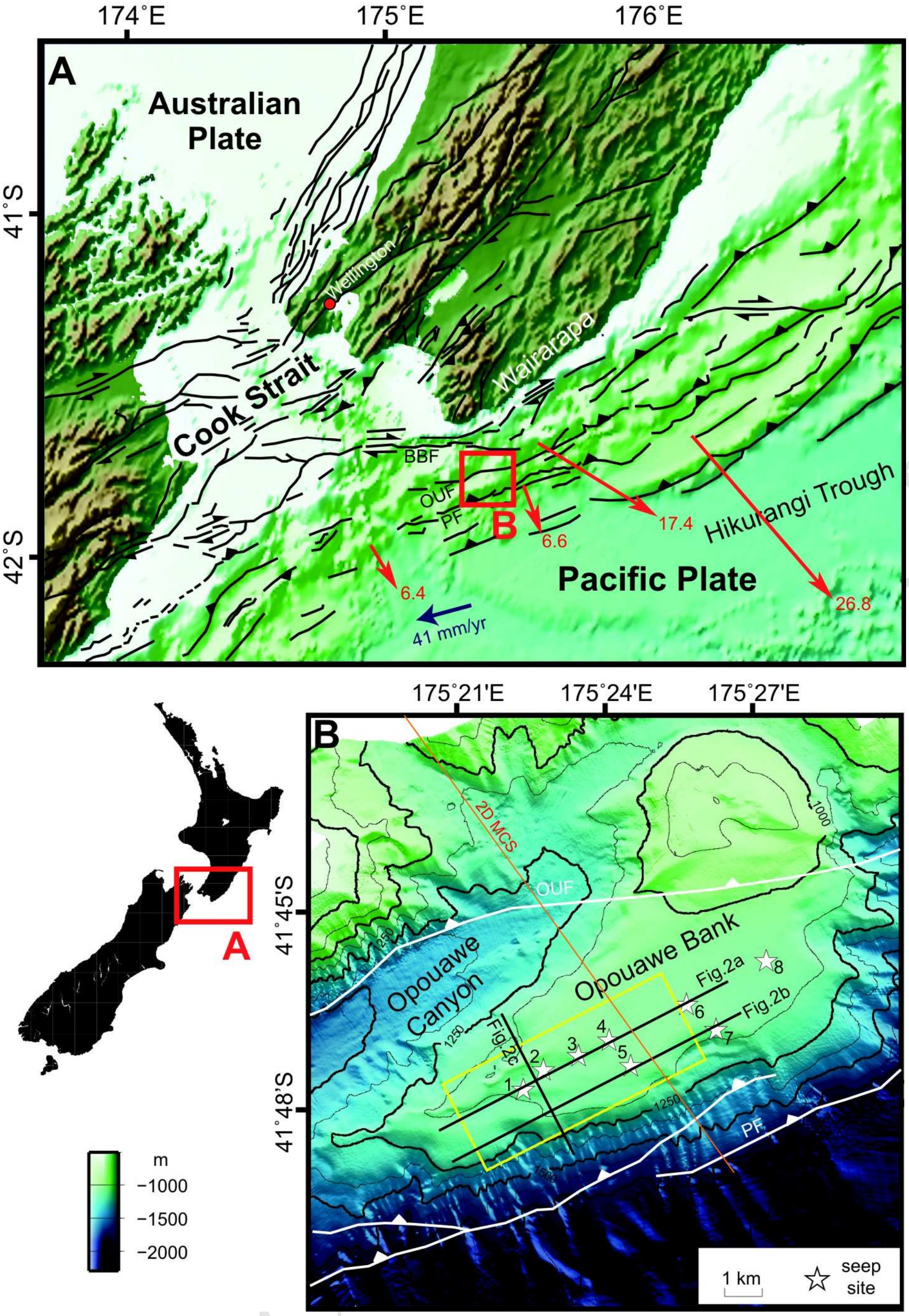

174˚E
175˚E
176˚E
41˚S
42˚S
A
Australian Plate
Wellington
Wairarapa
Cook Strait
BBF
OUF
PF
B
6.6
17.4
Hikurangi Trough
6.4
26.8
Pacific Plate
41 mm/yr
A
m
−1000
−1500
−2000
175˚21'E
175˚24'E
175˚27'E
41˚45'S
41˚48'S
B
2D MCS
1000
OUF
Opouawe Canyon
Opouawe Bank
Fig.2a
Fig.2b
Fig.2c
1250
1
2
3
4
5
6
7
8
PF
1 km
seep site

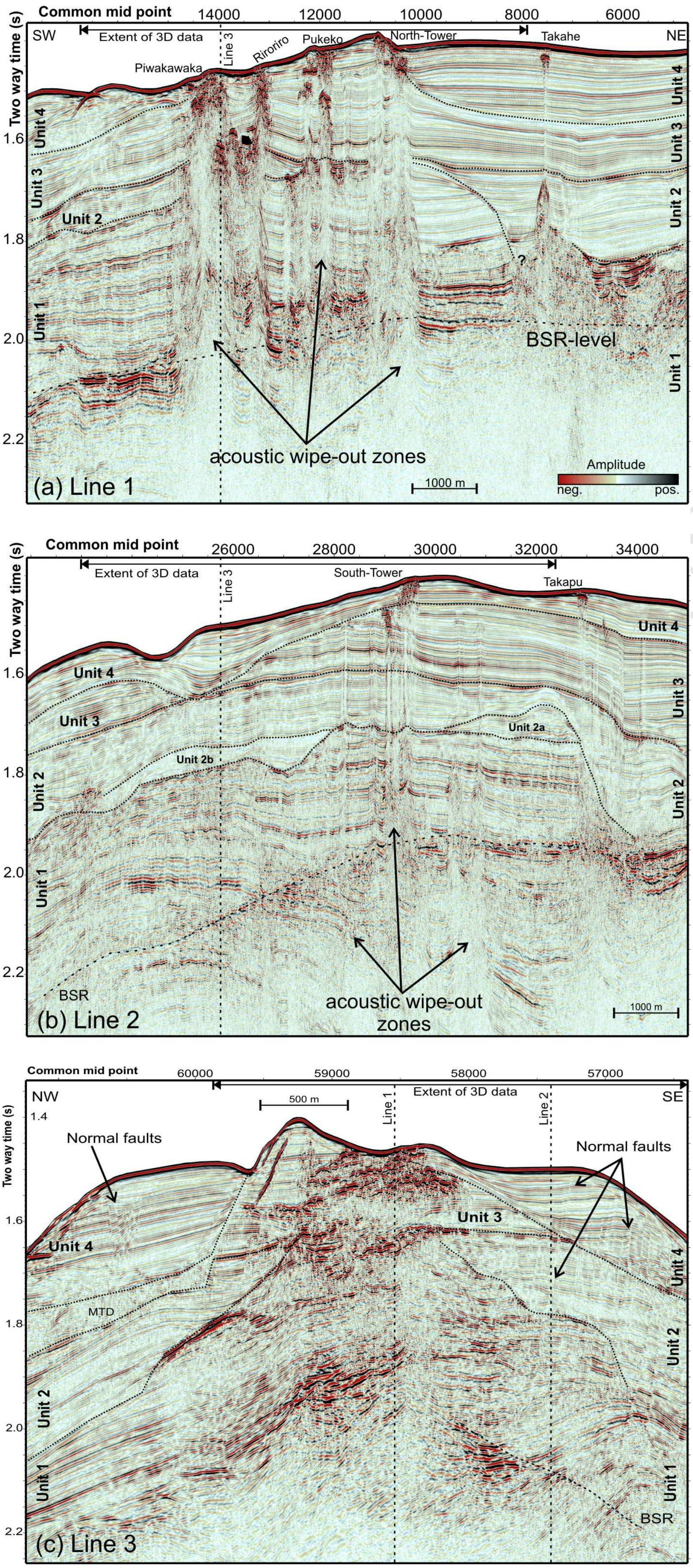
Common mid point
14000
12000
10000
8000
6000
Two way time (s)
SW
NE
Extent of 3D data
Line 3
Piwakawaka
Riroriro
Pukeko
North-Tower
Takahe
Unit 4
Unit 3
Unit 2
Unit 1
1.6
1.8
2.0
2.2
?
BSR-level
acoustic wipe-out zones
Amplitude
neg.
pos.
1000 m
(a) Line 1
Common mid point
26000
28000
30000
32000
34000
Two way time (s)
Extent of 3D data
Line 3
South-Tower
Takapu
Unit 4
Unit 3
Unit 2a
Unit 2b
Unit 2
Unit 1
1.6
1.8
2.0
2.2
BSR
acoustic wipe-out zones
1000 m
(b) Line 2
Common mid point
60000
59000
58000
57000
NW
SE
500 m
Line 1
Extent of 3D data
Line 2
1.4
Two way time (s)
Normal faults
Normal faults
Unit 3
Unit 4
MTD
Unit 2
Unit 1
1.6
1.8
2.0
2.2
BSR
(c) Line 3

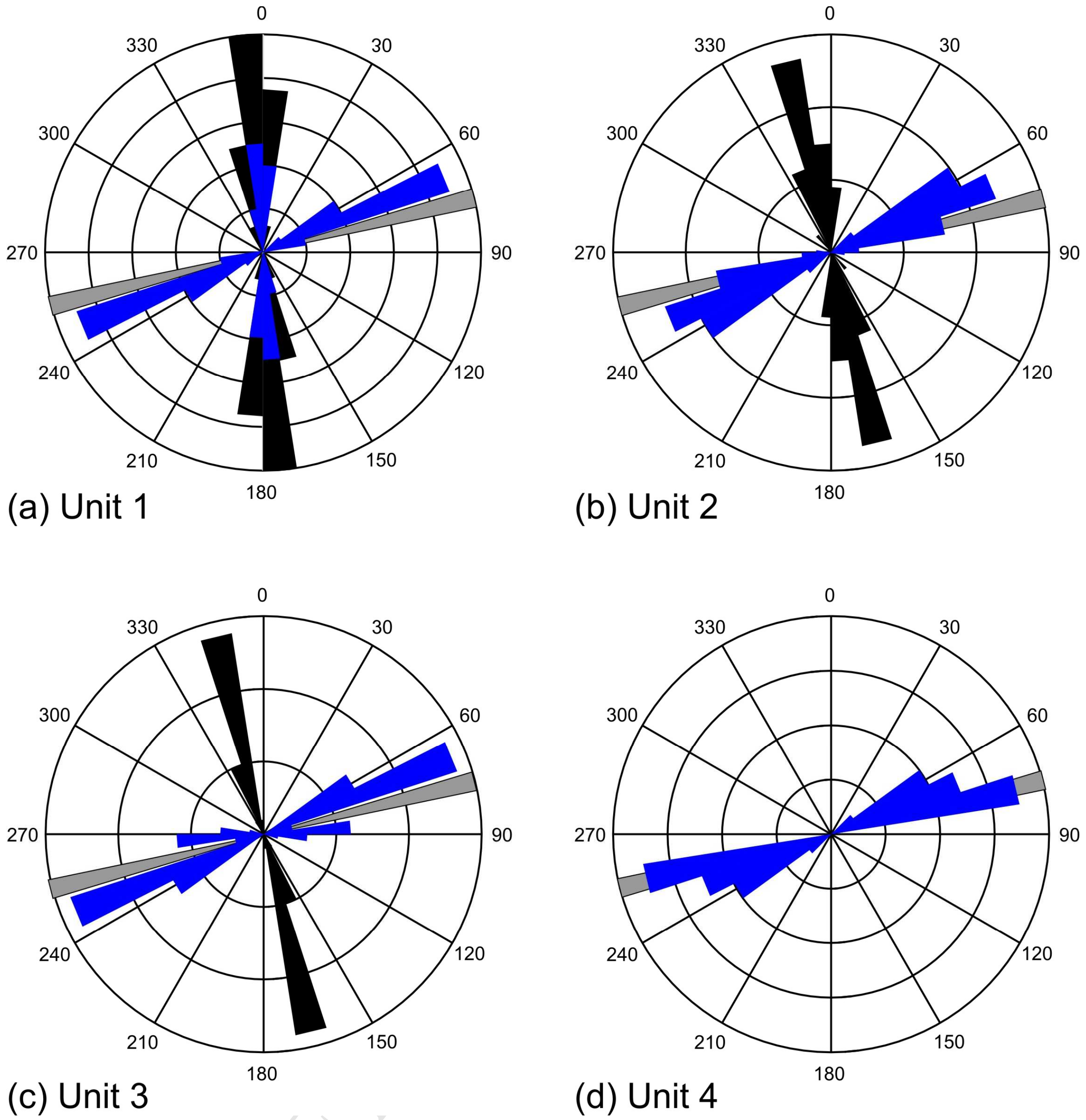
0
30
60
90
120
150
180
210
240
270
300
330
(a) Unit 1
(b) Unit 2
(c) Unit 3
(d) Unit 4

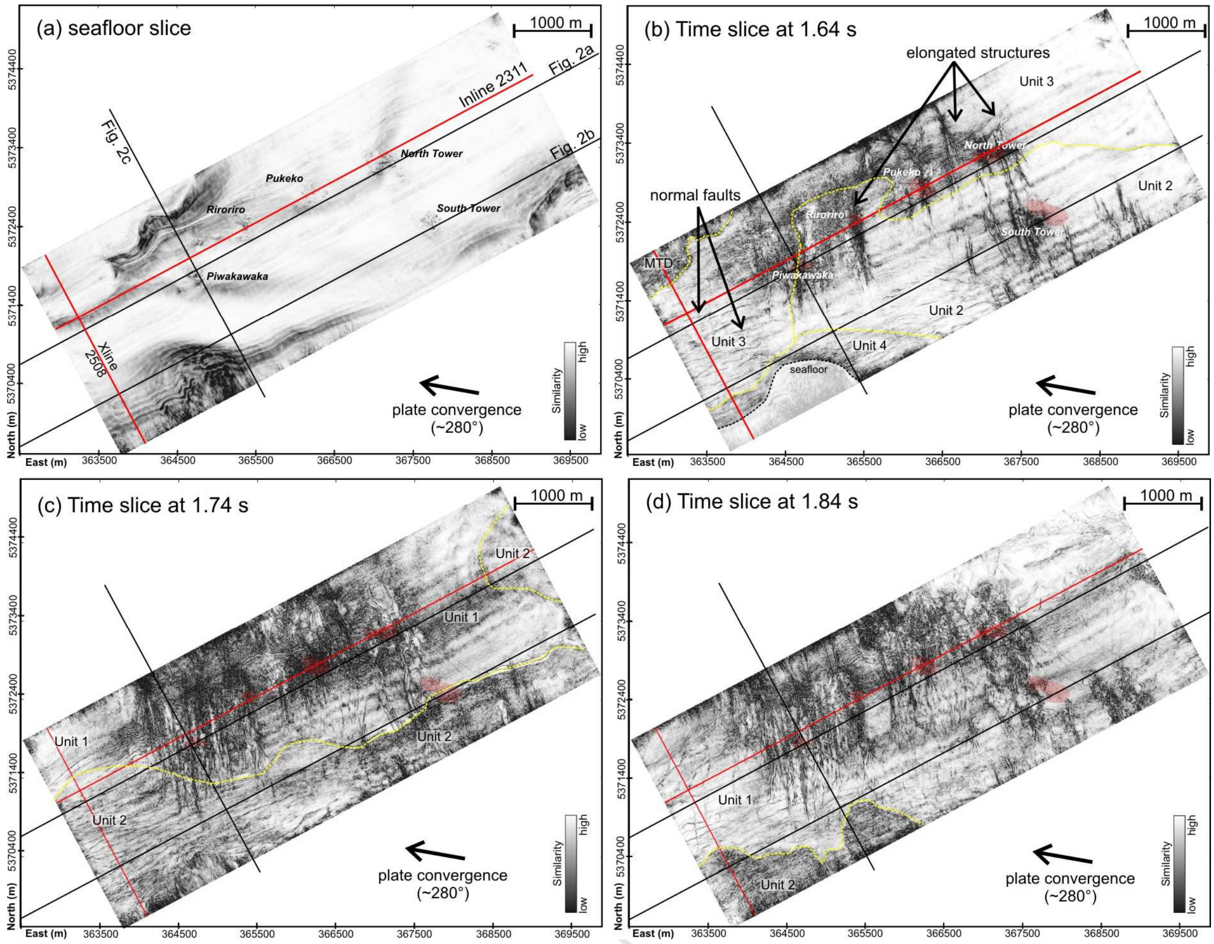
(a) seafloor slice
1000 m
Inline 2311
Fig. 2a
Fig. 2b
Fig. 2c
Pukeko
North Tower
Riroriro
South Tower
Piwakawaka
Xline 2508
plate convergence (~280°)
Similarity
high
low
(b) Time slice at 1.64 s
elongated structures
Unit 3
normal faults
MTD
Unit 2
Unit 4
seafloor
(c) Time slice at 1.74 s
Unit 1
Unit 2
(d) Time slice at 1.84 s
North (m)
East (m)
363500
364500
365500
366500
367500
368500
369500
5370400
5371400
5372400
5373400
5374400

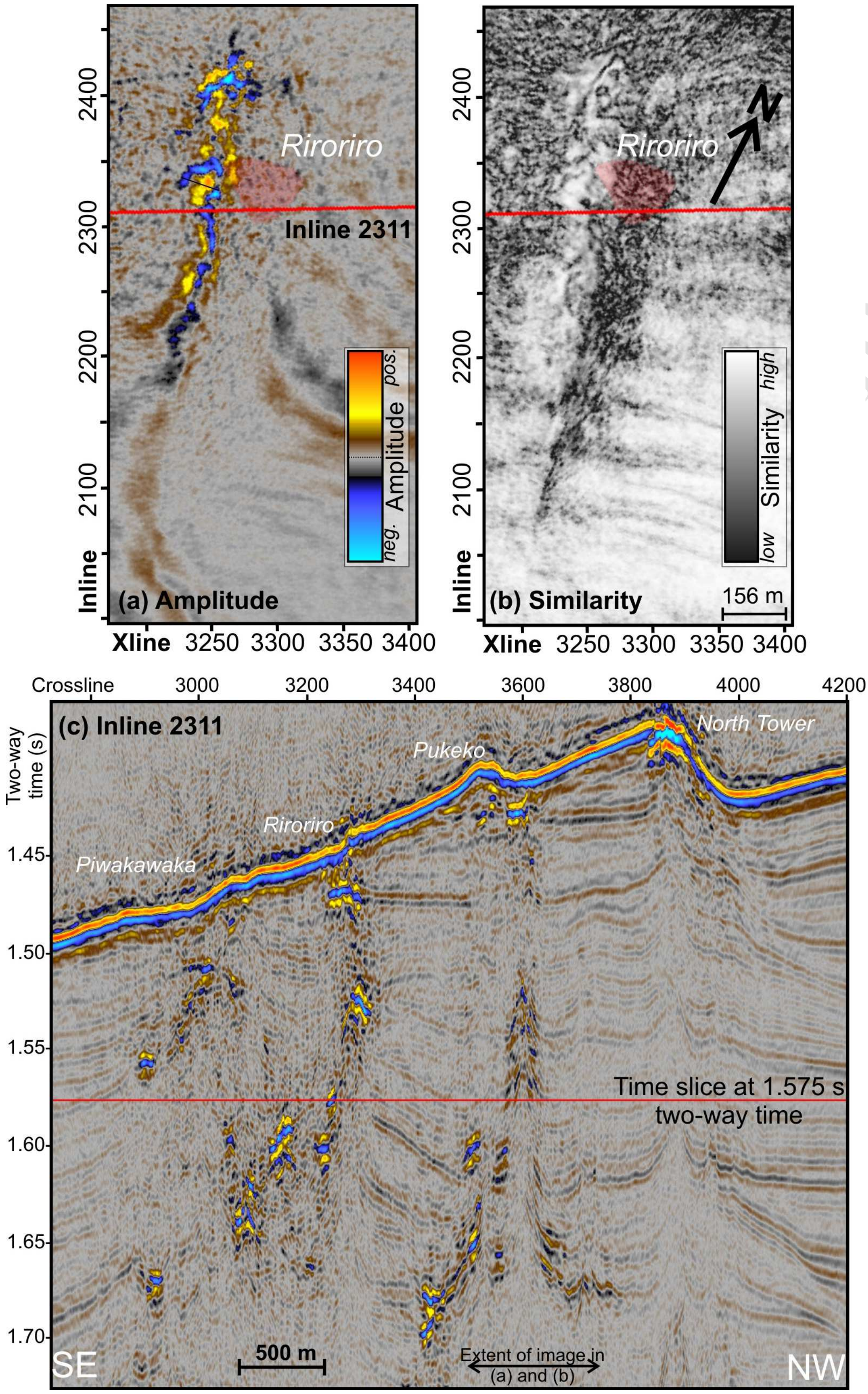

Riroriro
Inline 2311
pos.
Amplitude
neg.
Inline
(a) Amplitude
Xline 3250 3300 3350 3400
2400
2300
2200
2100
Riroriro
N
high
Similarity
low
(b) Similarity
156 m
Xline 3250 3300 3350 3400
Crossline 3000 3200 3400 3600 3800 4000 4200
(c) Inline 2311
Two-way time (s)
North Tower
Pukeko
Riroriro
Piwakawaka
1.45
1.50
1.55
1.60
1.65
1.70
Time slice at 1.575 s two-way time
SE
500 m
Extent of image in (a) and (b)
NW

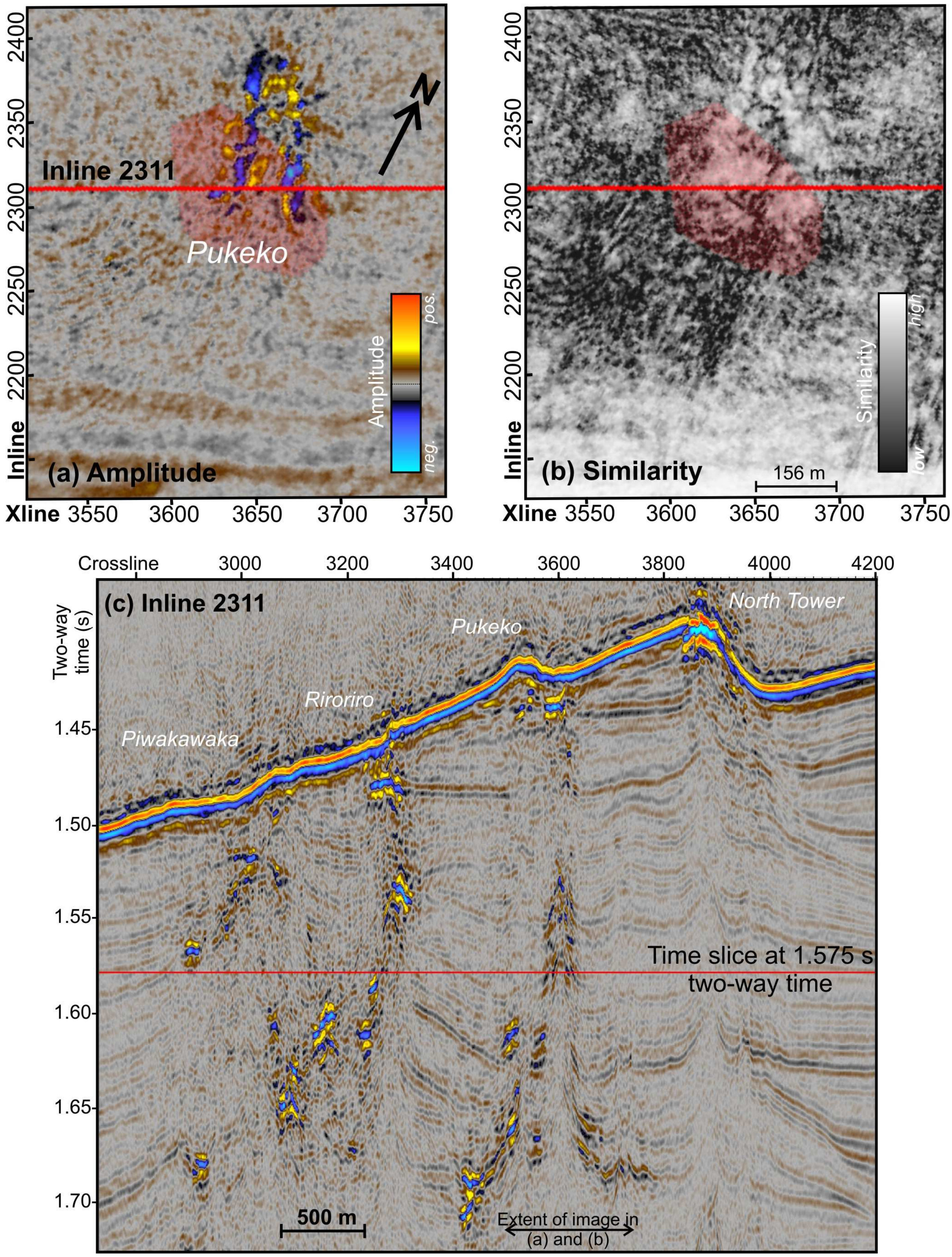

Inline 2311
Pukeko
N
(a) Amplitude
Amplitude
pos.
neg.
Inline
2400
2350
2300
2250
2200
Xline 3550 3600 3650 3700 3750
(b) Similarity
Similarity
high
low
156 m
Crossline 3000 3200 3400 3600 3800 4000 4200
(c) Inline 2311
Two-way time (s)
1.45
1.50
1.55
1.60
1.65
1.70
Piwakawaka
Riroriro
Pukeko
North Tower
Time slice at 1.575 s two-way time
500 m
Extent of image in (a) and (b)

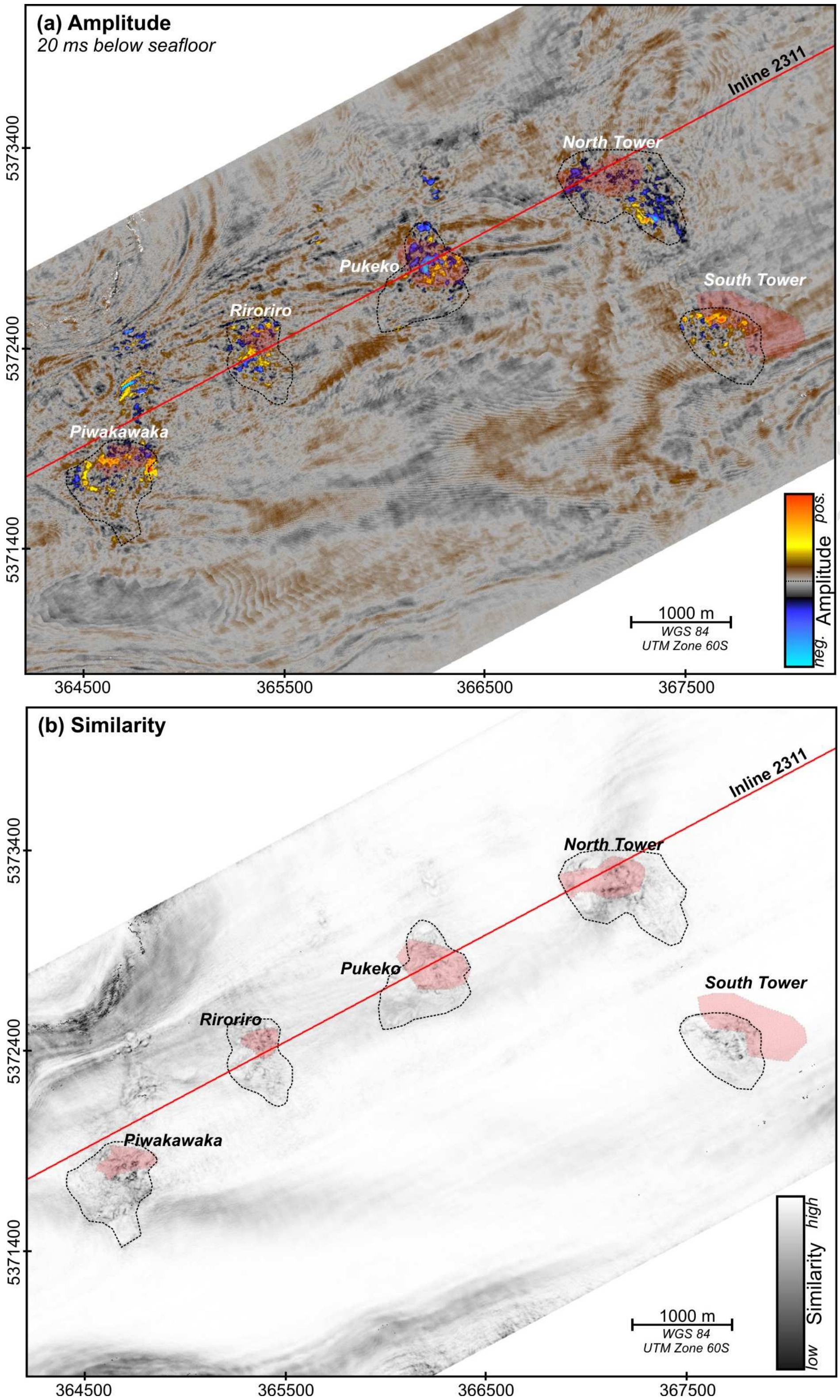
(a) Amplitude
20 ms below seafloor
Inline 2311
North Tower
Pukeko
South Tower
Riroriro
Piwakawaka
5373400
5372400
5371400
364500
365500
366500
367500
1000 m
WGS 84
UTM Zone 60S
neg. Amplitude pos.
(b) Similarity
Inline 2311
North Tower
Pukeko
South Tower
Riroriro
Piwakawaka
5373400
5372400
5371400
364500
365500
366500
367500
1000 m
WGS 84
UTM Zone 60S
low Similarity high

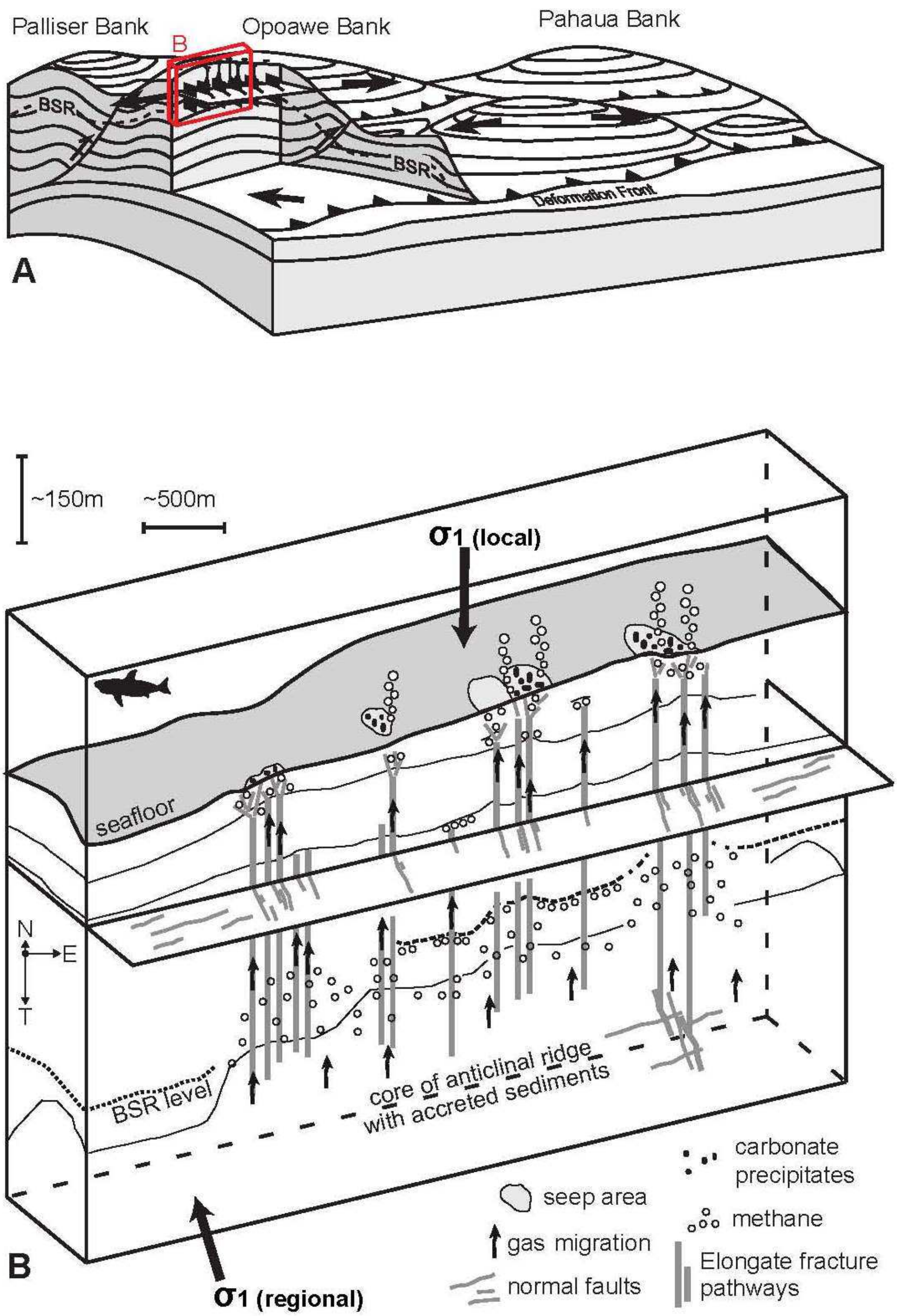
Palliser Bank
Opoawe Bank
Pahaua Bank
B
BSR
BSR
Deformation Front
A
~150m
~500m
σ1 (local)
seafloor
N
E
T
BSR level
core of anticlinal ridge
with accreted sediments
carbonate
precipitates
seep area
methane
gas migration
normal faults
Elongate fracture
pathways
B
σ1 (regional)

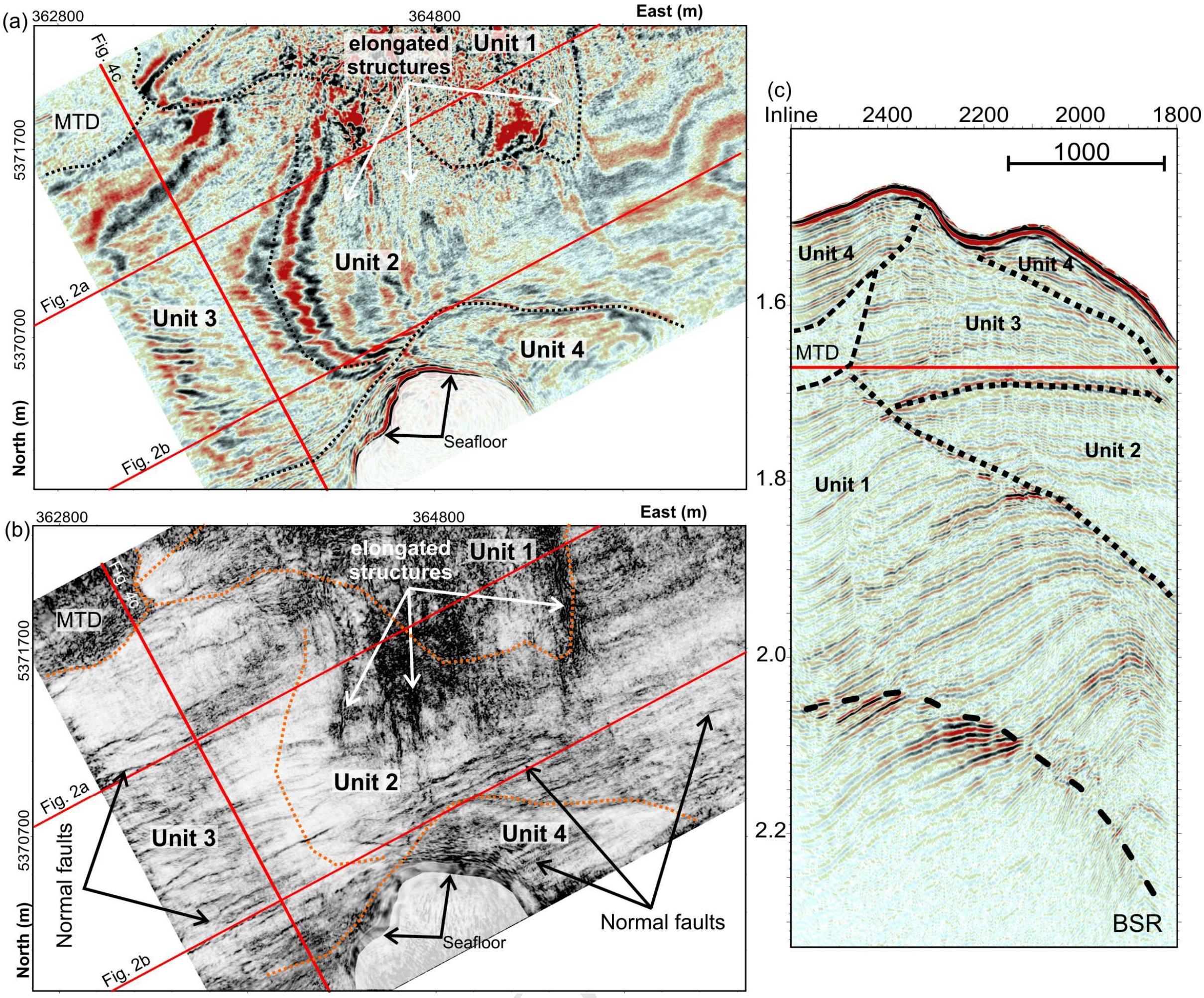
(a)
362800
364800
East (m)
5371700
5370700
North (m)
Fig. 4c
MTD
elongated structures
Unit 1
Unit 2
Unit 3
Unit 4
Fig. 2a
Fig. 2b
Seafloor
(b)
362800
364800
East (m)
5371700
5370700
North (m)
MTD
elongated structures
Unit 1
Unit 2
Unit 3
Unit 4
Fig. 2a
Fig. 2b
Normal faults
Seafloor
Normal faults
(c)
Inline
2400
2200
2000
1800
1000
1.6
1.8
2.0
2.2
Unit 4
Unit 4
Unit 3
MTD
Unit 2
Unit 1
BSR

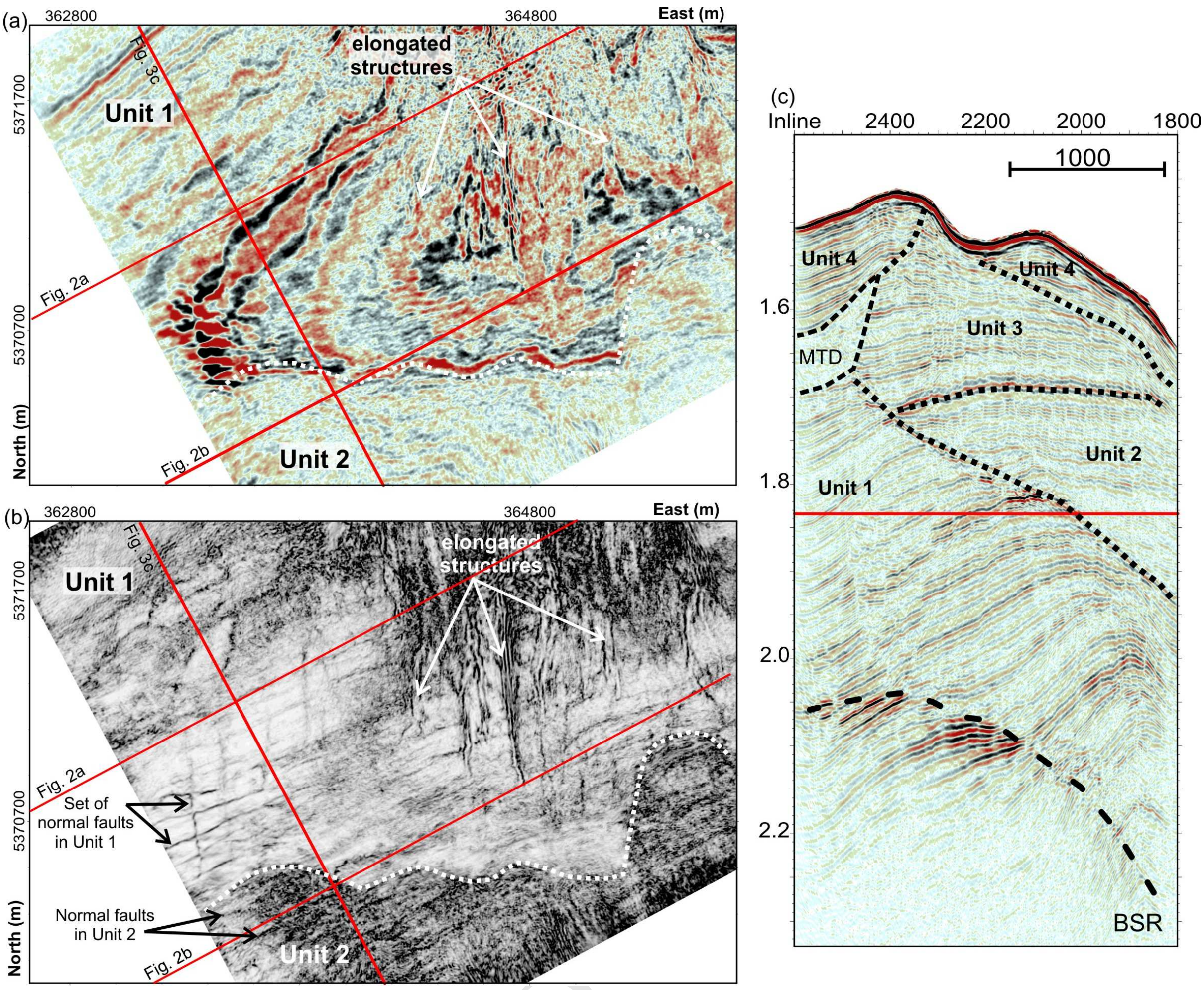

(a)
362800
364800
East (m)
5371700
5370700
North (m)
Fig. 3c
Unit 1
elongated structures
Fig. 2a
Fig. 2b
Unit 2
(b)
362800
364800
East (m)
5371700
5370700
North (m)
Unit 1
Fig. 3c
elongated structures
Fig. 2a
Set of normal faults in Unit 1
Normal faults in Unit 2
Fig. 2b
Unit 2
(c)
Inline
2400
2200
2000
1800
1000
Unit 4
Unit 4
1.6
Unit 3
MTD
Unit 2
1.8
Unit 1
2.0
2.2
BSR

Highlights to manuscript:

"Elongate fluid flow structures: Stress control on gas migration at Opouawe Bank, New Zealand" by Michael Riedel, Gareth Crutchley, Stephanie Koch, Christian Berndt, Joerg Bialas, Gerald Eisenberg-Klein, Jürgen Prüßmann, Cord Papenberg, and Dirk Klaeschen

- Elongated fault structures are conduits for focused fluid flow
- Gas migration occurs only along a sub-set of faults across Opouawe bank
- Stress state deduced from 3D fault structures appears partially stratigraphically controlled